Sedimentology and stratigraphic architecture of a fluvial to shallow-marine succession: the Jurassic Dhruma Formation, Saudi Arabia

BASSAM ALSHAMMARI[a,b], NIGEL P. MOUNTNEY[a], LUCA COLOMBERA[a], MOHAMMED A. AL-MASRAHY[b]

[a] *Fluvial, Eolian & Shallow-Marine Research Group, School of Earth and Environment, University of Leeds, LS2 9JT, UK*

[b] *Exploration Organization, Saudi Aramco, Dhahran 31311, Saudi Arabia*

ABSTRACT

The interaction of fluvial, tidal, and wave processes in coastal and paralic environments gives rise to sedimentary successions with highly varied styles of facies architecture; these are determined by the morphology and evolutionary behavior of the range of coastal sub-environments, which may be difficult to diagnose in subsurface sedimentary successions with limited well control.

This study presents depositional models to account for stratigraphic complexity in a subsurface fluvial to shallow-marine succession, the Middle Jurassic Dhruma Formation, Saudi Arabia. The study achieves the following: (i) it examines and demonstrates sedimentary relationships between various fluvial, nearshore, and shallow-marine deposits; (ii) it develops depositional models to account for the stratigraphic complexity inherent in fluvial to shallow-marine successions; and (iii) it documents the sedimentology and the stratigraphic evolutionary patterns of the lower Dhruma Formation in the studied area of Saudi Arabia. The dataset comprises facies descriptions of 570 m of core from 14 wells, 77 representative core thin sections, 14 gamma-ray logs, and FMI image logs from 4 wells. These data are integrated with quantitative information from > 50 analogous systems from a wide range of modern and ancient settings, stored in a relational database. Stratigraphic correlations reveal the internal anatomy of the succession.

Facies associations are representative of fluvial channels, intertidal flats, pedogenically modified supratidal flats or floodplains, river-influenced tidal bars, weakly storm-affected shoreface and offshore-transition zones, storm-dominated delta-front and prodelta settings, and an open-marine carbonate-dominated shelf. These sub-environments interacted in a complex way through space and time. The vertical succession of the studied interval records an overall transition from coastal-plain deposits at the base to marine deposits at the top. As such, the succession records a long-term transgressive, deepening-upward trend. However, this general trend is punctuated by repeated progradational events whereby coastal sand bodies of fluvial, wave, and tidal origin prograded basinward during stillstands to fill bays along a coastline. The nature of juxtaposition of neighboring sub-environments has resulted in a sedimentary record that is highly complex compared to that generated by morphologically simple shoreface systems that accumulate more regularly ordered stratal packages.

KEYWORDS

Fluvial, Shallow marine, Mixed-energy coastal system, Mixed siliciclastic and carbonates, Iron ooids.

INTRODUCTION

Coastal fluvial to shallow-marine settings comprise a range of environments including estuaries, lagoons, tidal flats, strandplains, barrier islands, beaches, and deltas; these pass basinward into marine offshore settings. Shoreline environments are defined and further subdivided by the relative importance of fluvial, wave, and tidal processes (Boyd et al., 1992; Harris et al., 2002). These environments are commonly classified using various simple yet widely employed ternary classifications on the basis of dominant and subordinate process regimes (Galloway, 1975; Johnson and Baldwin, 1986; Boyd et al., 1992; Porebsky and Steel, 2006; Ainsworth et al., 2011).

The interaction of fluvial, tidal, and wave processes in nearshore coastal environments gives rise to the accumulation of depositional bodies that are represented in the sedimentary record by a variety of types of architectural elements (Miall, 1985; Olariu et al., 2012; Vakarelov and Ainsworth, 2013). The internal facies architecture and external preserved geometry of these sedimentary units is determined by the morphology and the evolutionary behavior of the range of formative coastal sub-environments (Dalrymple et al., 2003). The coastal terminus of rivers, where many of the aforementioned physical processes interplay, is termed the fluvial-to-marine transition zone (FMTZ), wherein there typically exists a downstream transition from fluvial dominance to marine dominance (Dalrymple and Choi, 2007; Van den Berg et al., 2007; Gugliotta et al., 2019). This zone can extend for tens to hundreds of kilometers upstream from shorelines at the lower reaches of rivers. Examples of studies that document such reaches include: the present-day Fraser River delta, western Canada (Dashtgard et al., 2012), the Fly River delta, Papua New Guinea (Dalrymple et al., 2003), and the Amazon River, Brazil (Dalrymple et. al., 2015). The influence of fluvial processes can also extend for hundreds of kilometers seaward from the shoreline in front of the river mouths during episodes of high river discharge (Dalrymple and Choi, 2007 and Gugliotta et al., 2019). Several studies have investigated depositional processes operating in this region, including documentation of the gravity-flow deposits of the Fraser River delta front associated with fluvial and tidal interaction (Ayranci et al., 2012), and remote-sensing analysis of the outward delta plume of the Mekong River (Loisel et al., 2014). In recent years, a growing number of studies have examined the detailed sedimentology of FMTZ-related deposits, from both modern systems (e.g., La Croix and Dashtgard, 2014; La Croix and Dashtgard, 2015, Prokocki et al., 2015; Gugliotta et al., 2017; Gugliotta et al., 2019) and from ancient successions (e.g., Van den Berg et al., 2007; Shiers et al., 2014; Martinius et al., 2015; Gugliotta et al., 2016; La Croix et al., 2019a).

In shallow-marine settings – given appropriate combinations of latitude, climate, water depth, and a limited supply of nutrients and clastic detritus – carbonate deposition may occur in parts of systems that are elsewhere dominated by clastic sedimentation (Vicalvi and Milliman, 1977).

Sand bodies present in various accumulations of fluvial to shallow-marine origin are known in the subsurface chiefly through drill-core and seismic data records. Examples of successions representative of fluvial to shallow-marine sub-environments (including those of the FMTZ) include the Triassic Mungaroo Formation, NW Shelf, Australia (Heldreich et al., 2017), the Jurassic Brent Group, North Sea, UK (Livera and Caline, 1990), the Cretaceous McMurray Formation, Alberta, Canada (Hubbard et al., 2011; Hein, 2015; Jablonski and Dalrymple, 2015), and the Cretaceous Burgan Formation, Kuwait (Al-Eidan et al., 2001). In these settings, sand-body accumulations can be laterally extensive over kilometers where they represent large-scale depositional elements (Wightman and Pemberton, 1997; Shchepetkina et al., 2016; Reynolds, 2017). However, although sand-prone overall, these types of successions tend to be internally lithologically heterogeneous at a variety of smaller scales, for example as exemplified by sandstone beds partitioned by thin but numerous mudstone interbeds (e.g.,

Reineck and Wunderlich, 1968; Reineck and Singh, 1980; Thomas et al., 1987; Nio and Yang, 1991). As such, developing detailed sedimentological models of fluvial to shallow-marine successions known only from the subsurface is challenging (Jackson et al., 2005; Martinius et al., 2005; Ringrose et al., 2005; Massart et al., 2016). Gaining an improved understanding of the sedimentary facies distribution and anatomy of these types of deposits is therefore important for subsurface characterization. A key part of this is the development of predictive lithofacies models (Dalrymple and Choi, 2007; Burton and Wood, 2013; Al-Masrahy and Mountney, 2015; Dashtgard and La Croix, 2015; Al-Masrahy, 2017; Van de Lageweg et al., 2018) based on observations of the lateral extent and continuity of architectural elements in the subsurface, as inferred from subsurface data including cores, wireline logs, seismic data, and, in some cases, pressure data. Nonetheless, it remains a difficult task to reconstruct the geometry and continuity of sandstone bodies representative of fluvial to shallow-marine settings from subsurface data alone. Uncertainty associated with attempts to characterize subsurface successions can be reduced by utilizing analogues based on studies of outcrops and modern systems, and from which quantitative measures of facies and architectural-element proportions, geometries, and distributions can be obtained (e.g., Ainsworth et al., 2008, 2011; Colombera et al., 2012, 2016a).

The aim of this study is to document the nature of interaction in fluvial to shallow marine systems. Specific objectives are as follows: (i) examine and demonstrate the relationships between various fluvial, nearshore, and shallow-marine deposits, (ii) construct depositional models to account for the stratigraphic complexity inherent in fluvial to shallow-marine successions, and (iii) document the sedimentology and the stratigraphic evolutionary patterns of the lower Dhruma Formation in the studied area of Saudi Arabia. The aim and objectives are fulfilled through the consideration of a subsurface dataset from the lower Dhruma Formation in Saudi Arabia (Fig. 1; exact well locations cannot be published due to the proprietary nature of the dataset, though well positions relative to one another are indicated). The dataset enables the characterization of sedimentary geobodies considered to represent fluvial to shallow-marine paleoenvironments and allows prediction of the occurrence and arrangement of those geobodies in the subsurface.

GEOLOGICAL SETTING

The Arabian plate, which formed part of the northeastern margin of the Gondwana supercontinent, experienced diastrophic tectonic events throughout much of its geological history (Haq et al., 1988; Haq and Al-Qahtani, 2005; Faqira et al., 2009; Stewart, 2016). In the Permian, it was located at approximately 25° south of the paleoequator, before it progressively shifted northwards during the Triassic and Jurassic (Scotese, 2001; Ziegler, 2001; Schlaich and Aigner, 2017) to occupy a position close to the equator during the Mesozoic (Stampfli and Borel, 2002; Golonka, 2007; Seton et al., 2012; Stewart et al., 2016). This shift of position was accompanied by events that influenced the geology of the Arabian Plate. In the late Permian, the Neo-Tethys Ocean started to form as a result of continental rifting and spreading between the Zagros suture and Gulf of Oman. This led to the formation of a northeast-dipping passive margin (Ziegler, 2001). In the Early Jurassic, back-arc rifting commenced along the eastern Mediterranean basin, and this induced uplift in the western and southern parts of the Arabian plate. This resulted in the development of a new northward-dipping passive margin to the Neo-Tethys Ocean, with an associated open-marine shelf paleoenvironment (Ziegler, 2001).

The surface geology of the region is presently covered with aeolian sand dunes, except for bedrock exposures that crop out in the western part of the basin near the Arabian Shield (Fig. 1). The subsurface succession records the basin fill of an elongate basin that plunges to the northeast from south of the Arabian Shield towards the United Arab Emirates (Soliman and Al-Shamlan, 1980; Haq et al., 1988; Tawfik et al., 2016). The study region is bounded by the Qatar Arch to the north and northwest, and by the Hadhramaut-Oman arches to the south and southeast.

In the fill of the studied basin, the lower part of the Middle Jurassic Dhruma Formation is the focus of this study. The Dhruma Formation was first identified in outcrop and was originally assigned as a member of the Tuwaiq Mountain Formation by Max Steineke in 1937 (summarized in Powers et al., 1966), but was subsequently ranked as a formation in its own right by Brankamp and Steineke (Arkell, 1952). Later workers have subdivided the Dhruma Formation into Lower, Middle, and Upper members based on distinct lithological changes recognized in outcrop (Powers et al., 1966; Powers, 1968). More recently, the formation has been further subdivided into seven informal units: lowermost D1 to uppermost D7 (Vaslet, et al., 1983; Enay et al., 2009). Where exposed in outcrop, the lower Dhruma Formation is subdivided to units D1 and D2, which are referred to in the literature as the Balum Member and the Dhibi Limestone Member, respectively (Al-Husseini, 2009).

In the subsurface, the lower Dhruma Formation of the study area is composed dominantly of a siliciclastic accumulation of coastal-plain and shallow-marine origin, equivalent to the D1 unit (or the Balum Member seen in outcrop). This siliciclastic succession passes vertically to a carbonate-dominated succession, which forms the upper part of the lower Dhruma Formation (equivalent to the D2 unit, Dibi Limestone Member seen in outcrop). The lower Dhruma Formation was reported to represent marginal-marine to paralic environments by Stewart et al. (2016) as part of their review of the Mesozoic subsurface succession. However, no detailed and systematic sedimentological lithofacies analysis of the formation has been published previously.

DATA AND METHODS

Subsurface Datasets

This study integrates techniques in lithofacies analysis, ichnology, and sequence stratigraphy based on analysis of subsurface data from 14 wells that penetrate the lower Dhruma Formation in the studied area, in Saudi Arabia. The dataset includes subsurface core data, representative thin sections from core, gamma-ray logs, and image logs. Cores and thin sections have been described in detail in terms of grain-size distribution, grain texture (clast shape, sorting), sedimentary structures, bed thickness, bed contact types, and bioturbation intensity using the bioturbation index scale (Taylor and Goldring, 1993). Using these descriptive criteria, thirteen distinct lithofacies are identified in the succession. These lithofacies are grouped into five principal facies associations that have been interpreted as being representative of vertical accumulations arising in response to particular suites of depositional processes; each facies association is considered representative of sedimentation in a particular paleoenvironment.

Based on correlations between the studied wells, three stratigraphic cross sections (correlation panels) have been constructed, two in an orientation considered close to parallel to the depositional strike of the sedimentary system, and one along a dip-oriented profile. These three panels have been used to determine the spatial distribution of the defined facies associations. Correlation has been undertaken principally based on analysis of the sedimentary logs and the gamma-ray signatures. Well-log gamma-ray data from the studied wells were placed against the descriptive sedimentary core logs to account for the uncored sections of the lower Dhruma Formation. Logs and cores are commonly mismatched with respect to reported depths due to the tools stretching because of high temperature in the deep boreholes (Crain, 2015). To address discrepancy between the reported depths of the sedimentary logs (descriptions of the cores) and the gamma-ray logs, a standard core-to-log calibration technique has been applied by matching the core gamma-ray logs (as obtained in the laboratory after cutting the core) with the reference (wireline) gamma-ray logs. This typically required a core shift of up to 7 m downward or upward with respect to the reference gamma-ray log. The gamma-ray signature, which is a proxy for sand and shale in the subsurface, was used to derive insight into vertical lithology trends. The gamma-ray signature of the uncored intervals has

been interpreted based on the gamma-ray log responses typical of different depositional settings. For example, the bell-shaped gamma-ray signatures correspond to channel-fill deposits and the funnel-shaped ones correspond to prograding marine shelf or delta-front deposits (cf. Emery and Myers, 1996). Age-diagnostic palynomorphs, described by Stewart et al. (2016), were considered in this study to discriminate the relevant successions of the Middle Jurassic lower Dhruma Formation from the underlying lower Jurassic and/or Upper Triassic formations. FMI image-log analyses (results provided courtesy of Shahzad Ulhaq, Saudi Aramco) from four wells have also been used to determine the paleoflow direction of the defined geobodies (e.g., dip directions of sedimentary structures of different types).

Constraining Uncertainty Associated with Inter-Well Correlation

This study is based primarily on a comprehensive one-dimensional subsurface dataset from wells distributed over an area of approximately 150 km x 150 km (Fig. 1B). The two wells that are closest to each other have a spatial separation of 4 km (wells 3 and 4), whereas the two most widely separated wells are ~ 126 km apart (wells 12 and 13). Therefore, there exists a degree of uncertainty.

In the subsurface study, cores and wireline-log signatures (gamma-ray logs) are the principal data types utilized to infer depositional environments. These types of data indicate the vertical extent of different geobodies, biostratigraphy content, and physical properties of the rock (porosity, permeability etc.), and provide relative age dates through biostratigraphy. However, determining the stacking patterns and the lateral connectivity of geobodies is not straightforward. Uncertainty can be associated with facies interpretation of gamma-ray signatures in cases where cores are unavailable. For example, shoreface and delta-front facies may display similar characteristics and may be difficult to discriminate using well-log data alone.

Geobody geometry has been estimated by employing appropriate modern and ancient analogues from which distributions of geobody length and width can be derived; estimates of geobody lateral extent can be attempted based on knowledge of their thickness. Analogue data were obtained from a relational database detailing sedimentary architectures: the Shallow Marine Architecture Knowledge Store (SMAKS) (Colombera et al., 2016a). The SMAKS database has here been used to provide quantitative information on the architectures and dimensions of geobodies for ancient shallow-marine and paralic siliciclastic successions deemed analogous to the subsurface Dhruma Formation. The database was filtered and queried to derive analog data that are the most suitable to this study. For example, data relating to sedimentary units that represent only one part of a tidal flat (i.e., sand flat or mud flat) were disregarded, as tidal-flat deposits described in this study include a full suite of sand flats, mixed flats, and mud flats. Moreover, data on parasequence-scale shoreface sandstones (cf. Colombera and Mountney, 2020a, 2020b), and on shallow-marine sandstones more generally were considered. Examples of such deposits were filtered on their thicknesses to ensure that only those that are comparable in scale to those observed in core were considered. Relationships between the thickness and lateral dip extent of sedimentary units (i.e. facies associations) as obtained from SMAKS, have been considered to guide well correlations in the studied subsurface succession.

RESULTS

Fourteen distinctive lithofacies types have been identified from the analyzed cores of the lower Dhruma Formation (Table 1). These have been grouped into five main facies associations based on their arrangement and genetic relations to one another. The five facies associations are categorized as follows: fluvial channels (FA1); intertidal flats and pedogenically modified

supratidal or floodplains (FA2); river-influenced tidal bars (FA3); shoreface and delta (FA4); and open-marine and shelf carbonates (FA5). Facies associations FA2, FA4, and FA5 have been further subdivided into two sub-associations each. Representative graphical sedimentary log examples from which facies associations have been identified are shown in Figure 2.

Fluvial-Channel Deposits (FA1)

Description.--- This facies association was observed in 7 wells (see Table 2) and commonly has an erosional base and occurs on top of FA2. FA1 is composed of fining-upward packages of massive (Sm) and cross-bedded sandstone (Sx) that always pass upward to thinner beds of heterolithic mudstone and sandstone (Hms) and mudstone (Ms). These deposits are sand dominated and occur as a single package (e.g., middle of well 12 in Fig. 2), else as repeated cyclically arranged packages (e.g., top of well 1 and base of well 12 in Fig. 2). A single package of strata representing this facies association is 0.5 to 4 m in thickness. The sandy units are commonly thicker (0.2 to 3.5 m) than the overlying heterolithic facies (0.1 to 0.8 m). The sandstone units exhibit erosional bases that are commonly overlain by lag sediments (Lg), mainly of very coarse sand grains and mud pebbles (Fig. 3A, B) whereas the overlying heterolithic and mudstone facies show gradational or sharp bases. There also exists rare small-scale (0.2 m) alternating sandstone (Sx) and heterolithic facies (Hms) towards the upper part of the overall sandy section (Fig. 3C).

Generally, the sandstone facies grade upward into planar-bedded medium- to fine-grained sandstone and siltstone units. The massive and cross-bedded sandstone consistently has sparse floating mud chips (1.2 to 5 mm diameter) present in it, as well as sparse clasts of organic and coaly debris (Fig. 3A, B). FA1 exhibits millimeter-scale, carbonaceous laminae draping the cross-stratified sets in wells 10, 12 and 13. These laminae are faint in the lower parts of the sandy units but more pronounced upwards. Localized double mud drapes occur in well 13 at the transition between the sandstone and the overlying heterolithic facies (Fig. 3D). The heterolithic units in this association are mud-dominated (mainly clay) and contain thin beds and lenses of sand (Fig. 3E) and common wavy to lenticular bedding. They cap and/or separate units composed of the sandy facies (Fig. 3C, D, E). Localized vertical burrows (*Skolithos*) are observed at the upper contact of sandstone units that are directly overlain by the heterolithic facies; these burrows likely originate at the interface with the overlying finer-grained sediments. In the heterolithic facies, small sporadic forms of *Planolites* and other unidentified burrows are present. The heterolithic facies is commonly overlain by the deposits identified in FA2b (Fig. 3F).

Interpretation.---The numerous erosional beds indicate repeated high-energy currents eroding the underlying sediments. The massive coarse sandstone with lack of pronounced sedimentary structures and bioturbation suggests rapid deposition by deceleration of high-energy, heavily sediment-laden currents (Martin, 1995; Collinson et al., 2006; Dalrymple et al., 2015). The abundance of clasts of mudstone, organic matter, and coaly debris suggests reworking of pre-existing sediments, and perhaps transportation by fluvial currents. The vertical trend of the succession, with lag sediments resting on an erosional base and passing upward into massive sandstone, is a characteristic that is common of channel-fill deposits (Martini and Aldinucci, 2017). The more cyclic occurrence of thick sandstone overlain by thin intervals of heterolithic deposits is interpreted to represent alternation of high and low river flow stages. The thick sandstone units were likely deposited during river-flood periods (high river discharge), whereas the overlying heterolithic interval was likely deposited during inter-flood periods (low river discharge) (Dalrymple et al., 2015). Possible tidal effects are indicated by the presence of double mud drapes in well 13. Overall, this facies association is interpreted to represent fluvial-channel and overbank deposits. The fluvial-channel deposits observed in well 13 with the possible tidal effect may represent deposition in the upstream region of the FMTZ.

Intertidal and Pedogenically Modified Supratidal Flat or Floodplain (FA2)

Intertidal-Flat Deposits (FA2a)

Description.--- This facies association was observed in eight wells (see Table 2). It was observed at the bottom of the formation, where cored, across much of the study area. It unconformably overlies the lower Jurassic carbonate deposits of the upper Marrat Formation. This facies association overlies the fluvial deposits of FA1 in many wells. It mainly consists of fining-upward packages (up to 5 m thick with an average of ~ 3 m) of heterolithic fine- to medium-grained muddy sandstone that transitions to sandy mudstone facies (mainly clay) (Hms). The sandy part contains cross-lamination and stacked symmetric bidirectional ripple forms (Collinson and Mountney, 2019) that decrease in frequency and become isolated towards the muddy part (Fig. 4A). Unidirectional ripples also exist in the sandy facies. Repeated double mud drapes are observed in various parts in this facies association (Fig. 4A). It also shows common flaser, wavy, and lenticular bedding as well as abundant thin, very fine sand lenses in the finer interval (Fig. 4B). Distorted beds locally occur at the bottom of the sandstone facies. In places, shrinkage cracks are observed in the muddy parts of this facies association. They taper downward and have infills of sediment derived from the bed above. Low to intense bioturbation is observed in sand-to-mud alternations, with bioturbation index values ranging from 1 to 5 (Fig. 4C). Identified ichnoforms include *Ophiomorpha*, *Planolites* and *Diplocraterion*.

Interpretation.---The presence of sand-to-mud alternation in the form of bidirectional rippled sandstone, together with the flaser, wavy, and lenticular bedding, suggests deposition during fluctuating energy levels (Reineck and Wunderlich 1968; Ginsburg 1975; Klein 1985). In this context, sand grains are typically deposited as bedload during the more energetic flows of a tidal cycle, generating bidirectional ripple forms (Boggs, 1995). By contrast, mud particles, possibly flocculated, settle out of suspension on the underlying rippled sand during low-velocity flows or at slack water, giving rise to the occurrence of flaser, wavy, and lenticular bedding (Klein, 1985; Boggs, 1995). The unidirectional ripple forms may represent deposition by ebb- or flood-dominant currents. Alternatively, the unidirectional ripples can possibly be products of fluvial currents. The observed shrinkage cracks are interpreted to be desiccation cracks that resulted from periodic subaerial exposure of the muddy deposits in the upper intertidal zone (Dalrymple, 2010). They are not likely to be syneresis cracks, given their downward-tapering form and fill of sediment derived from above (Collinson and Mountney, 2019). The vertical succession of this facies association, with its fining-upward trends, is similar to those interpreted as deposition in channel-related tidal flats (e.g.,Dalrymple, 2010; Desjardins et al., 2017). Overall, this facies association may represent channel-related tidal flat setting which dominated by tidal process. If the unidirectional ripple forms are of fluvial origin, the tidal flat setting may be within the inner FMTZ.

Pedogenically Modified Supratidal Flat or Floodplains (FA2b)

Description.--- This facies association was observed in nine wells (see Table 2). The heterolithic mudstone and sandstone of FA2a and those defined in FA1 repeatedly transition upward to thick (a few meters to 10 m) intervals of greenish-gray non-stratified very fine sandstone, siltstone, and mudstone (Sd), with intensive rooting (Fig. 4D). It also shows variegated mottling in some wells, with a brownish-red color interchanging with a greenish-gray color (Fig. 4E). In the highly oxidized facies, there exists centimeter-scale blocky volume that is separated by millimeter-scale iron-rich matrix (Fig. 4E). This non-stratified facies commonly shows thin beds of coal (~ 20 to 80 mm) (Fig. 4F, G), coarse- to pebble-size coal clasts and organic debris, and up to 0.8-m-thick coaly mudstone beds (Cm). Pyrite nodules and disseminated grains are observed in this FA and are associated with the presence of coal and organic material. Furthermore, thin sections of this facies indicate high content of kaolinite, and

organic and carbonaceous material (Fig. 4H, I). A low diversity of ichnogenera, mostly *Planolites*, is observed with a bioturbation index that ranges from 1 to 3.

Interpretation.---The non-stratified nature of this facies association suggests post depositional alteration to the sediments before lithification. The presence of rootlets across most of the facies suggests subaerial exposure which facilitated colonization by plants. Kaolinite is commonly formed during intense chemical weathering in warm and humid climate conditions (Weaver, 1989; Robert and Chamley, 1991); its high abundance in this facies association suggests that FA2b deposits were subjected to intense chemical alteration. The variegated form of red and brown colors suggests oxidation of iron-bearing sediments, possibly during subaerial exposure (Bromley, 1975; Pemberton and Frey, 1985; Pemberton et al., 1992; MacEachern et al., 1992, 2012). Pedogenic processes are also indicated by the presence of the blocky volumes that is separated by iron-rich matrix which suggest soil formation. Coaly debris and organic material observed in this facies association in most of the locations may have been reworked from localized vegetated swamps. This facies association is interpreted as subaerially exposed supratidal deposits in the seaward position of the region (wells 1, 2, 4, 5, 7, 8) and may represent altered floodplain deposits in more landward positions (wells 10, 12).

River-Influenced Tidal Bars (FA3)

Description.--- This facies association was observed in 3 wells (see Table 2) and observed overlying and underlying the intertidal and supratidal deposits of FA2. The facies association is composed of normally graded, centimeter- to decimeter-beds of non-stratified very coarse to medium quartz-dominated sandstone (Sm), commonly with scoured bases overlain by coarse-grained lag sediments (Lg). This massive sandstone shows relatively thicker beds (0.4 m on average) and with more frequent erosional bases in well 11 compared to wells 3 and 4 where the massive beds are 0.10 m on average. It generally grades upward to stacked sets of medium-grained trough and planar cross-bedded sandstone (Sx). Sedimentary structures observed in Sx include planar cross-stratification, with foresets that possess thin (up to 5 mm) single and double mud drapes (mainly clay). Sand and mud couplets were also observed within bundles (Fig. 5A). Furthermore, the cross-stratified sets are observed bounded by unbioturbated erosional surfaces (reactivation surfaces). In Sx, there exist thin beds (20 to 40 mm) of non-stratified very coarse sandstone that generally grade upwards to coarse and medium grain size (Fig. 5B, C). These are commonly overlain by cross-bedded sandstone with double mud drapes (Fig. 5C). The double mud drapes occur more frequently towards the top of the sandy part of FA3. Towards the top of FA3, heterolithic (Fig. 5D) and non-stratified facies (Fig. 5E) were observed overlying the sandstone facies. The heterolithic and non-stratified facies are similar to those observed in FA2. Thin sections record limited presence of kaolinite in Sx (Fig. 5F, G). Bioturbation is generally rare in FA3. This facies association exhibits a high proportion of carbonaceous and organic material.

Interpretation.--- Single and double mud drapes, reactivation surfaces, and sand–-mud couplets are considered as possible tidal indicators (Visser, 1980; Dalrymple and Choi, 2007; Dalrymple, 2010; Davis, 2012). Mud drapes typically represent deposition from suspension during low-velocity tidal flow or at slack-water periods (Visser, 1980), whereas reactivation surfaces indicate pause planes (discontinuities in sedimentation) or reversing tidal currents (Boersma and Terwindt, 1981). Alternation of sand and mud beds in the form of bundles is commonly described as the product of flood and ebb tidal cycles (Visser, 1980). However, recent work demonstrates that such bundles may originate in tide-modulated fluvial settings (Martinius and Gowland, 2011) or in purely fluvial settings (Ainsworth et al., 2011). The thin, normally graded beds indicate deposition by high-energy currents possibly by fluvial currents. The overlying double mud drapes and their upward increase in frequency of occurrence supports an interpretation of increasing tidal influence over time. The coaly fragments, organic

material, and kaolinite present in this facies association imply reworking of sediments from a coeval adjacent vegetated setting.

This facies association indicates interaction of tidal and fluvial currents. Tidal currents are interpreted to be the dominant controlling process overall, though significant fluvial influence is evident in places. Overall, the deposit of FA3 are interpreted as river-influenced tidal bars in a potentially estuarine setting.

Shoreface to Offshore Transition and Delta-Front to Prodelta (FA4)

Weakly Storm-Affected Shoreface to Offshore-Transition Zone (FA4a)

Description.--- This facies association was cored in eight wells (see Table 2), where it consistently overlies the oolitic ironstone of FA5b. This facies association comprises amalgamated coarsening- and thickening-upward packages (0.5 m to a few meters thick) of massive mudstone (partly calcareous), heterolithic mudstone and sandstone (Hms), and fine- to medium-grained hummocky cross-stratified sandstone (Shcs) and bioturbated sandstone (Sd). These packages show increasing proportion of sand upwards. The mudstone units (Ms) are homogeneous, with rare pronounced sedimentary structures. The heterolithic part is composed of mudstone and very fine- to fine-grained sandstone and exhibits an upwards increase in sand proportion (Fig. 6A). Local slightly asymmetrical lenticular ripples were observed in the heterolithic unit (Fig. 6B). In facies Hms, rare thinly laminated sandstone beds with erosional bases are present in places. In its upper part, FA4a is dominated by the presence of weakly to intensely bioturbated, dominantly fine-grained sandstone of Sb (Fig. 6C), which commonly grades up to cleaner (relatively lower mud content) lightly bioturbated sandstone with apparent hummocky cross-stratification (Shcs). The bioturbated sandstone is composed of poorly sorted grains and shows rare preserved cross bedding. Abundant rounded to elongate, concentrically lined iron-rich ooids are scattered in various parts of this facies association (Fig. 6D). A slightly diverse assemblage of ichnogenera is present in FA4a: *Skolithos*, *Planolites*, *Ophiomorpha*, and *Teichichnus*; the bioturbation index varies from 2 to 5.

Interpretation.---The coarsening-upwards packages of mudstone, heterolithic strata, and sandstone indicate increasing energy levels as a result of decreasing depositional water depth (Van Wagoner et al. 1990 and Howell et al., 2008). The defined ripple forms observed are likely products of wave activity above fair-weather wave base where propagating waves produce a slight landward shift of sediment forming the asymmetrical shape (Reineck and Singh, 1980). The observed intensity and diversity of bioturbation present in FA4a successions suggest broad organism colonization, in low-energy settings (e.g., Pemberton et al. 2003). The decrease in bioturbation in the sandstone facies and the presence of hummocky cross-stratification is attributed to periods of storm wave activity, likely between the fair-weather and the storm wave bases (Harms et al., 1975; Collinson and Mountney, 2019). Variations in bioturbation may also reflect changes in sedimentation rate, whereby organisms colonize the sediments during periods of low sedimentation rate (Bromley, 1996). The abundance of iron-rich ooids in this facies association is attributed to reworking of pre-existing ooids. Overall, this facies association is interpreted as a prograding storm-affected offshore-transition zone to shoreface environment.

Storm-Dominated River-Influenced Prodelta to Delta-Front Deposits (FA4b)

Description.--- This facies association was observed only in well 2; however, gamma-ray signatures in two nearby wells (wells 3 and 4) show striking resemblance with the corresponding gamma-ray signatures of well 2. FA4b was observed overlying the open-marine carbonate deposits of FA5a in two coarsening- and thickening-upwards packages (that are ~ 9 and 10 m thick). These packages consist of mudstone (Ms), heterolithic mudstone and sandstone (Hms), and fine to medium-grained sandstone (Sx and Shcs). The mudstone unit is blocky and homogeneous in nature. The mudstone facies (Ms) shows numerous fine sandstone lenses and thin to medium beds (up to 150 mm) of thinly laminated very fine sandstone,

commonly with erosional bases, and exhibit moderate to weak bioturbation (BI:1 to 3) (Fig. 6E, F). These deposits grade up to faintly laminated to low-angle cross-bedded fine to medium-grained sandstone (Sx) and hummocky and swaly cross-stratified fine to medium-grained sandstone (Shcs) (Fig. 6G, H). The facies association becomes more sand-dominated upwards. Furthermore, several inversely graded beds (50 to 120 mm) are observed with well-rounded medium to angular grains, floating mud chips and rare preserved gastropod shells. These beds occur towards the upper parts of the sandstone units. The sandstone units are composed primarily of quartz grains with common interstitial greenish chlorite cement (Fig. 6J). Bioturbation is generally rare in the sandstone units, but a low diversity of ichnogenera (e.g., diminutive forms of *Planolites*, *Skolithos,* and fugichnia) was observed in Sx, disturbing the original sedimentary structures.

Interpretation.---Similar to FA4a, FA4b deposits are indicative of increasing energy levels, likely associated with a decrease in water depth, which is recorded by the coarsening- and thickening-upwards trends. The mud in Ms and Hms in the lower part of each package generally suggests deposition from suspension under quiet water conditions. Periods of storm events eroding the muddy substrate are indicated by the presence of numerous erosionally based sandy beds and lenses (Baniak et al., 2014). The bioturbated heterolithic strata are indicative of storm power fluctuations (cf. Collins et al., 2020). Hummocky and swaly cross-strata present in this facies association are typically wave-generated structures (e.g., Harms et al., 1975; Meene et al., 1996). The inverse grading that occurs towards the upper parts of the sand-dominated units may indicate deposition by hyperpycnal flows during waxing river discharge (Bhattacharya and MacEachern, 2009). The overall scarcity of bioturbation indicates environmental conditions that prevented organisms from flourishing. Such conditions might have been due to high rates of sediment influx into the system, freshwater input, and/or high-energy wave currents (MacEachern et al., 2007a, 2007b). The local presence of low-index and low-diversity ichnogenera assemblages observed in the sand units is attributed to periods of lower wave action and/or lower sedimentation rate, which might have enabled the temporary activity of organisms (Bromley, 1996; Pemberton et al., 2012). Subsequent episodes of high rates of sedimentation would have required the organisms to escape upward to reach the water-substrate interface (Pemberton and MacEachern, 1997; Bann et al., 2008; MacEachern and Bann, 2008, Pemberton et al., 2012). The observed ichnofossil assemblage represents an impoverished and distal expression of the *Skolithos* ichnofacies (MacEachern and Bann, 2008). Overall, this facies association is interpreted to have formed in a prograding storm-dominated river-influenced delta-front to prodelta setting (cf. Collins et al., 2020).

Open-Marine Shelf (FA5)

Carbonate Shelf (FA5a)

Description.--- This facies association was observed in three wells (see Table 2). It forms the lower part of the two packages defined in FA4b in well 2 and marks the top of the cored section in wells 7 and 11. Packages of carbonate facies overlie FA4b and FA4a in well 2 and FA4b in wells 7 and 11. Generally, this association comprises limestone (Ls) that changes in composition and grain size upwards to calcareous mudstone (Msc). The limestone facies is grain dominated (packstone to grainstone; Dunham, 1962). The limestone facies occur as amalgamated bedsets of approximately 4 m thickness, or as thinner interbeds (50 to 150 mm) between packages of facies Msc. The grain composition includes common outsized quartz grains, abundant ooids, and shell and skeletal fragments that are commonly replaced by dolomite rhombs. At the base of the deepest occurrence of this limestone, ooids and skeletal grains are highly fragmented. This facies shows moderate to intense bioturbation (BI: 3 to 5) (Fig. 7A, B). The overlying mudstone beds are marly at their bases but become less calcareous toward their tops. Mudstone beds are blocky and show many drilling-induced fractures (Fig. 7C). In places mudstone beds reveal thin parallel lamination, and limited wavy to lenticular

bedding and can exhibit an increasing proportion of sand upwards. In addition, Msc shows scattered shell fragments in a clayey matrix. Bioturbation in Msc is generally sporadic and is developed most intensely near lithological boundaries. Unlike the limestone units observed in well 2, coarsening- and thickening-upward beds are preserved in wells 7 and 11 with smaller packages of mud-dominated to grain-dominated limestone (wackestone to grainstone). The grain types observed are primarily coated grains, ooids, intraclasts, and shell and skeletal fragments. Dolomite cement dominates the lower part of the section (Lsd), and decreases in abundance as it is replaced by calcite upwards.

Interpretation.---The calcite-rich sediments together with the abundant ooids, shells, and skeletal fragments indicate periods of carbonate sedimentation. The ooids formed in agitated shallow-water settings (Davies et al., 1978; Rankey and Reeder, 2012). The overall dominance of grainstone in the carbonate facies is indicative of high-energy shoal environments. The presence of skeletal and grain fragmentation at the base of the limestone in well 2 suggests reworking by high-energy currents to leave a lag deposit, possibly during transgression. The mudstone that occurs on top of the limestone is interpreted to be deposited from settling out of suspension in quiet water conditions, possibly during a subsequent flooding (i.e., deepening) event.

Iron-Rich Oolitic Shoal (FA5b)

Description.--- This facies association was observed in six wells (see Table 2). It is observed overlying the tidal-flat and supratidal deposits of FA2 and the fluvial channel deposits of FA1, with sharp bases. These deposits are always capped by the mudstone of FA4a. They show an overall fining-upward trends and consists primarily of calcareous sandstone (Sc), ooid-rich ironstone (Ore), and calcareous mudstone (Msc). The calcareous sandstone is carbonaceous and composed of poorly sorted fine to medium quartz grains with abundant bioclasts and scattered chamosite ooids (Fig. 7D, F). The ooid-rich ironstone is composed primarily of orange-brown ooids, skeletal fragments, and sparse detrital quartz grains that are of fine to medium sand size (Fig. 7E, G). The ooids show concentric laminae around various types of nuclei, including clay, quartz, and skeletal fragments. They are mostly rounded to slightly elongate in shape and are deformed in some instances (Fig. 7G). Some of these ooids are completely or partly dissolved and replaced by dolomitic rhombs. The calcareous mudstone is observed interbedded with and/or overlying the calcareous sandstone and the ooid-rich ironstone. The mudstone facies comprises sparse ooids and skeletal fragments at the base of beds; these decrease in abundance upward within beds.

Interpretation.---The dominance of ooids in this facies association indicates accumulation in high-energy, shallow-water settings (Chen et al., 2017). The iron in these accumulations could have been transported from the continent to the sea as Fe-bearing detritus or Fe-clay colloids by river currents (Maynard, 1983; Einsele, 2000). The calcareous sandstone with the abundant ooids and fragmented bioclasts also suggest reworking by wave activity in close proximity to a carbonate source. The stratigraphic position of this facies association, overlying the nearshore deposits of FA1 and FA2, and being overlain by marine deposits of FA4a, suggests deposition during a transgressive episode. This is in accord with how these types of ooidal ironstones are commonly interpreted to form under transgressive conditions (cf. Hallam and Bradshaw, 1979; Bayer et al. 1985; Van Houten 1985; La Croix et al., 2019b).

Paleocurrent Analysis

Subsurface cores do not reveal information required for paleocurrent identification, in that the cores are not oriented. Rather, image logs of the boreholes provide the prevalent type of data used to infer paleocurrent directions. In this study, Formation Micro Imager (FMI) logs acquired from four wells were used to interpret the paleocurrent directions for the defined facies associations. Interpretations of image logs are summarized in rose diagrams (Fig. 8), which

report the dip directions of foresets of cross-bedded sandstones from shoreface (FA4a) deltaic (FA4b), tidal-bar (FA3) and fluvial-channel (FA1) deposits. The foreset dip directions of the shoreface sandstone cross-bedded sets from well 8 and the deltaic sandstone from well 2 show broadly consistent north-northeast (present day) dip directions. Inclined forests of tidal-bar deposits also show a broad northeast dip direction with limited variability. This broad unidirectional bedding of tidal bars might indicate an ebb-dominant tidal current that is driven by dominant river input at the estuary mouth. However, the position of the tidal bars with respect to the channel remains uncertain. Overall, these observations indicate a broad northeastward progradation and direction of sediment dispersal. However, the dip directions of a fluvial channel interpreted from well 13 vary and indicate east, southeast, and northwest (present day) dip directions, which could be due to the formative channel being sinuous and/or to in-channel secondary, or possibly reversing, flow.

Spatial Distribution of Facies Associations

The studied cores are divided into two main facies belts: coastal-plain deposits comprising FA1, FA2, and FA3 facies associations, and marine deposits, including the FA4 and FA5 facies associations. To illustrate the spatial distribution of the facies, correlations between the defined facies associations have been performed across the study area, principally based on the available sedimentary log data and well log gamma-ray signatures, but also supported by secondary analog data from the SMAKS database; a data summary is provided in Figure 9. The three resulting correlation panels are shown in Figure 10A, B, C. The non-cored intervals have been interpreted based on their gamma-ray signatures, which typically yield information on the rock characteristics and enable lithological interpretations (Emery and Myers, 1996).

The data obtained from the SMAKS database show the relationship between thickness and dip length of numerous shoreface and shallow-marine sand belts, tidal bars and tidal flats. Thickness-dip-length relationships of shallow-marine sand belts (Fig. 9A) indicate that a 10 m thick sandstone (analogous to the sandstone observed in FA4b) ranges in dip length from a few hundreds of meters to nearly 40 km. Limited data related to tidal flats and tidal bars were obtained, from which a relationship cannot be obtained (Fig. 9B). However, some instances of meter-thick tidal flats can be several hundreds of meters long in dip direction, and may reach up nearly 2 km. For example, one 7.5-m-thick tidal bar is 1.5 km in dip length. These data have been applied to help constrain expected sand body architectures in the correlation panels of Figure 10.

Sections A-A' and B-B' have been constructed in an orientation approximately parallel to the depositional strike of the system. These sections show an overall vertical transition from a coastal-plain succession at the base to a marine succession at the top. Section A-A' (Fig. 10A) reveals a thicker succession of marine deposits overlying the coastal-plain deposits compared to cross section B-B' (Fig. 10B), which is itself interpreted to have occupied a position farther landward (towards the west) by virtue of a thicker coastal-plain succession and thinner marine succession. Section C-C' (Fig. 10C) has been constructed in an orientation approximately parallel to the depositional dip of the system (and intersecting panels A-A' and B-B'). This section reveals a dominance of coastal-plain deposits in the southwest of the area and predominantly marine deposits in the northeast. This section demonstrates an overall deepening-upward trend. However, six smaller-scale transgressive-regressive packages superimposed upon the overall deepening trend are identified. These packages are most clearly developed in the middle of section C-C' (Fig. 10C).

DISCUSSION

Controls on Sedimentation in the Lower Dhruma Formation

A depositional model depicting the evolution of the Middle Jurassic lower Dhruma Formation over five intervals is presented in Figure 11. Vertically, the study succession records an overall transition from coastal-plain deposits at the base to marine deposits at the top, as demonstrated in Figure 10A and B. The overall stratigraphic architecture of the lower Dhruma Formation is interpreted to be controlled by relative sea-level fluctuations, as well as by fluvial, tidal, and wave processes, as documented above.

The lower part of the section (interval 1) is dominated by fluvial and tidally influenced sedimentation, which resulted in the deposition of fluvial channel deposits (FA1), channel-associated tidal flats (FA2a), and river-influenced tidal bars. The deposits of FA2 and FA3 possibly represent deposition in the FMTZ in a mixed-energy estuary. Extensive paleosols (FA2b) are present across much of the study area; these indicate a prolonged period of subaerial exposure. This is overlain by two transgressive-regressive packages (interval 2). The transgressive components in these packages comprise reworked iron-rich oolitic shoal sediments (FA5b). The ooidal ironstone in this example is commonly interpreted to form from reworking of iron-rich coastal plains during transgressive events as documented above (cf. Bayer et al. 1985; Van Houten 1985). The regressive components are composed of progradational, weakly storm-affected offshore-transition-zone and shoreface units (FA4a). Interval 3 incorporates a package that is similar to those defined in interval 2, but with the transgressive component displaying reduced iron content in wells 2 and 5; this indicates the accumulation of carbonate sediments towards the northeast. Following the accumulation of interval 3, interval 4 is represented by two successive carbonate-mudstone-sandstone packages. The transgressive components of the two packages are represented by the fining-upwards limestone of FA5a. These are overlain by the regressive components represented by the prodelta and delta-front deposits of FA4b. These packages indicate two episodes of encroachment and retreat of carbonate-producing shelf areas. This is attributed to variations in the balance between the rate of relative sea-level change and the rate of supply of terrigenous sediment. Carbonate sedimentation developed most widely during episodes of limited siliciclastic influx or relative sea-level rise. By contrast, carbonate production was curtailed during episodes of increased rates of terrigenous sedimentation, or falls of relative sea level. The same factors acted to drive changes in shoreline position, which were paralleled by landward and basinward shifts in the foci of carbonate deposition (cf. Tirsgaard, 1996). Interval 5 incorporates the weakly storm-influenced shoreface deposits of FA4a in a more proximal position, farther southwest of the study area. These deposits are themselves overlain by carbonates that are apparently present across the entire study area.

Climate and Sediment Source

The Arabian Plate occupied a position near or at the equator during the Jurassic (Stampfli and Borel, 2002; Golonka, 2007; Seton et al., 2012; Stewart et al., 2016). Al-Aswad (1995) suggested that the climate of the Arabian Plate during the Jurassic was humid to semihumid. This has also been supported by the increased presence of small fern spores (Classopollis) along with an abundance of kaolinite in paleosols (e.g., Al-Hussaini, 2019). In the studied area, the defined supratidal or floodplain deposits also show enrichment of kaolinite, which is indicative of intense chemical alteration under a humid to semihumid climate (Weaver, 1989; Robert and Chamley, 1991).

The source of the clastic sediments of the Middle Jurassic succession has been interpreted by a number of authors. The eastern Mediterranean back-arc rifting in the Early Jurassic caused residual highs of western and southern parts of the Arabian Plate (Beydoun, 1991; Ziegler, 2001). In the Middle Jurassic, the Hadramaut-Oman Arches were the only elevated hinterlands

that could perhaps have acted as a source of sediments into various parts of the Arabian Peninsula, and which could have been drained by extensive channel networks (Al-Aswad, 1995). Al-Aswad (1995) suggests that southern central Arabia was traversed by alluvial tributaries draining the Hadramaut-Oman Arch, mainly from the south towards the north. The location of the study area and the broad northeastern paleoflow direction recorded in FMI image logs suggest that the siliciclastic sediments were likely sourced from the same southern Arabian hinterlands to the south and southwest.

CONCLUSIONS

A core-based sedimentological analysis of the Middle Jurassic lower Dhruma Formation in Saudi Arabia is presented. The study reveals that the lower Dhruma Formation was deposited in a varied range of fluvial to shallow-marine environments that interacted in a complex way over both space and time. Five lithofacies associations are identified based on the analysis of the core data; each is considered indicative of sedimentation within a particular paleoenvironment. The facies associations represent different paleoenvironments: fluvial channels, intertidal to pedogenically modified supratidal flats or floodplains, river-influenced tidal bars, deltaic and shoreface to offshore transition, and an open-marine carbonate-dominated shelf. The deposits of the facies associations are interpreted to be controlled by the interaction of fluvial, tide, and wave processes. At a larger scale, the pattern of sedimentation is controlled by the interplay of sea-level change and sediment accumulation rate, causing zones of sedimentation to shift with changes in the position of the paleoshoreline. The vertical successions of the lower Dhruma Formation record an overall transition from coastal-plain deposits at the base to marine deposits at the top. As such, the succession records a long-term transgressive, deepening-upward event. However, this overall deepening trend was punctuated by at least six progradational events whereby coastal deposits prograded basinward episodically.

ACKNOWLEDGMENTS

The authors would like to thank the Saudi Arabian Oil Company (Saudi Aramco) for funding this research and allowing this work to be published. We would like to thank our project partner Petrotechnical Data Systems (PDS) for provision of an academic license for Ava Clastics, which has been used to interrogate the Shallow-Marine Architecture Knowledge Store (SMAKS). We thank Marcello Gugliotta, Andrew La Croix, and an anonymous reviewer for their comments, which have significantly improved the article.

REFERENCES

Ainsworth, R.B., Flint, S.S., and Howell, J., 2008, Predicting coastal depositional style: Influence of Basin Morphology and accommodation/sediment supply regime within a sequence stratigraphic framework, *in* Hampson, G.J., Steel, R.J., Burgess, P.B., and Dalrymple, R.W., eds., Recent Advances in Shallow-Marine Stratigraphy: SEPM, p. 237-263.

Ainsworth, R.B., Vakarelov, B.K., and Nanson, R.A., 2011, Dynamic spatial and temporal prediction of changes in depositional processes on clastic shorelines: towards improved subsurface uncertainty reduction and management: American Association of Petroleum Geologists Bulletin, v. 95, p. 267-297.

Al-Aswad, A.A., 1995, Middle Jurassic non-marine siliciclastic facies in Southern Central Saudi Arabia: African Earth Sciences, v. 20, p. 253–262.

Al-Eidan, A.J., Wethington, W.B., and Davies, R.B., 2001, Upper Burgan Reservoir Description, Northern Kuwait: Impact on Reservoir Development: GeoArabia, v. 6, p. 179-208.

Al-Hussaini, A., Steel, R.J., Melvin, J., Olariu, C., Ertug, K., and Hooker, N., 2019, New evidence of regressing and transgressing Jurassic siliciclastic coastlines within the Dhruma Formation in Northern Central Arabia, Saudi Arabia: Sedimentary Geology, v. 379, p. 114–137.

Al-Husseini, M., 2009, Update to Late Triassic-Jurassic stratigraphy of Saudi Arabia for the Middle East geologic time scale: GeoArabia, v. 14, p. 145–186.

Al-Masrahy M.A., 2017, Modelling Temporal and Spatial Sedimentary Architectural Complexity in Mixed Aeolian-Fluvial Reservoir Successions: SPE-8802.

Al-Masrahy M.A., and Mountney N.P., 2015, Quantitative Approach to the Characterization of Sedimentary Architecture in Mixed Eolian-Fluvial Reservoir Successions: American Association of Petroleum Geologists, Search and Discovery, Article 41669.

Arkell, W.J., 1952, Jurassic ammonites from Jebel Tuwaiq, Central Arabia: Philosophical Transactions of Royal Society of London, Series B, Biological Sciences, v. 236, p. 241–313.

Ayranci, K., Lintern, D.G., Hill, P.R., and Dashtgard, S.E., 2012, Tide-supported gravity flows on the upper delta front, Fraser River delta, Canada: Marine Geology, v. 326, p. 166–170.

Baniak, G.M., Gingras, M., Burns, B., and Pemberton, S.G., 2014, An example of a highly bioturbated, storm-influenced shoreface deposit: Upper Jurassic Ula Formation, Norwegian North Sea: Sedimentology, v. 61, p. 1-25.

Bann, K.L., Tye, S.C., MacEachern, J.A., Fielding, C.R., and Jones, B.G., 2008, Ichnological and sedimentologic signatures of mixed wave- and storm-dominated deltaic deposits: examples from the early Permian Sydney Basin, Australia, *in* Hampson, G.J., Steel, R.J., Burgess, P.M., and Dalrymple, R.W., eds., Recent Advances in Models of Siliciclastic Shallow Marine Stratigraphy: SEPM, Special Publication 90, p. 293–332.

Bayer, U., Altheimer, E., and Deutschle, W., 1985, Environmental evolution in shallow epicontinental seas: sedimentary cycles and bed formation, *in* Bayer, W., and Seilacher, A., eds., Sedimentary and Evolutionary Cycles: New York, Springer-Verlag, p. 347-81.

Beydoun, Z.R., 1991, Arabian Plate Hydrocarbon Geology and Potential: A Plate Tectonic Approach: American Association of Petroleum Geologists, Studies in Geology, v. 33, 77 p.

Bhattacharya, J.P., and MacEachern, J.A., 2009, Hyperpycnal rivers and prodeltaic shelves in the Cretaceous seaway of North America: Journal of Sedimentary Research, v. 79, p.184-209.

Boersma, J.R., and Terwindt, J.H.J., 1981, Neap-spring tide sequences of intertidal shoal deposits in a mesotidal estuary: Sedimentology, v. 28, p. 151-170.

Boggs, S., Jr., 1995, Principles of Sedimentology and Stratigraphy, 2nd Edition: Upper Saddle River, New Jersey, Prentice Hall, 774 p.

Boyd, R., Dalrymple, R.W., and Zaitlin, B.A., 1992, Classification of clastic coastal depositional environments: Sedimentary Geology, v. 80, p. 139–150.

Bromley, R.G., 1975, Trace fossils at omission surfaces, *in* Frey, R.W., ed., the Study of Trace Fossils: A Synthesis of Principles, Problems, and Procedures in Ichnology: Berlin, Springer-Verlag, p. 399-428.

Bromley, R.G., 1996, Trace Fossils; Biology, Taphonomy and Applications, 2nd Edition: London, Chapman & Hall, 361 p.

Burton, D., and Wood, L.J., 2013, Geologically-based permeability anisotropy estimates for tidally-influenced reservoirs using quantitative shale data: Petroleum Geoscience, v. 9, p. 3-20.

Chen, L., Lu, Y.C., Fu, X.F., Xing, F.C., Wang, C., and Luo, C., 2017, Oolitic shoal complexes characterization of the lower Triassic Feixianguan Formation in the Yuanba gas field, northeast Sichuan Basin, China: Marine and Petroleum Geology, v. 83, p. 35–49.

Collins, D.S., Johnson, H.D., and Baldwin, C.T., 2020, Architecture and preservation in the fluvial to marine transition zone of a mixed-process humid-tropical delta: Middle Miocene Lambir Formation, Baram Delta Province, north-west Borneo: Sedimentology, v. 67, p. 1-46.

Collinson, J.D., and Mountney, N.P., 2019, Sedimentary Structures, 4th Edition: Edinburgh, Dunedin Academic Press, 340 p.

Collinson. J.D., Mountney N.P., and Thompson, D.B., 2006. Sedimentary Structures, 3rd Edition: Edinburgh, Dunedin Academic Press, 292 p.

Colombera, L., and Mountney, N.P., 2020a, On the geological significance of clastic parasequences: Earth-Science Reviews, v. 201, p. 103-062.

Colombera, L., and Mountney, N.P., 2020b, Accommodation and sediment-supply controls on clastic parasequences: a meta-analysis: Sedimentology, online, v. 67, p. 1667-1709.

Colombera, L., Felletti, F., Mountney, N.P. and McCaffrey, W.D., 2012, A database approach for constraining stochastic simulations of the sedimentary heterogeneity of fluvial reservoirs: American Association of Petroleum Geologists, Bulletin, v. 96, p. 2143-2166.

Colombera, L., Mountney, N.P., Hodgson, D.M., and McCaffrey, W.D., 2016a, The Shallow-Marine Architecture Knowledge Store: a database for the characterization of shallow-marine and paralic depositional systems: Marine and Petroleum Geology, v. 75, p. 83–99.

Colombera, L., Shiers, M.N., and Mountney, N.P., 2016b, Assessment of backwater controls on the architecture of distributary-channel fills in a tide-influenced coastal-plain succession: Campanian Neslen Formation, USA: Journal of Sedimentary Research, v. 86, p. 476-497.

Crain, E.R., 2015, Crain's Petrophysical Handbook [Online]: [Accessed 11 October 2019], Available from https://www.spec2000.net/.

Dalrymple, R.W., and Choi, K., 2007, Morphologic and facies trends through the fluvial-marine transition in tide- dominated depositional systems: a schematic framework for environmental and sequence stratigraphic interpretation: Earth-Science Review, v. 81, p. 135–174.

Dalrymple, R.W., 2010, Tidal depositional systems, in James, N.P., and Dalrymple, R.W., eds., Facies Models 4: Geological Association of Canada, p. 201–231.

Dalrymple, R.W., Baker, E.K., Harris, P.T., and Hughes, M.G., 2003, Sedimentology and stratigraphy of a tide-dominated, foreland-basin delta (Fly River, Papua New Guinea), *in* Sidi,

F.H., Nummedal, D., Imbert P., Darman H., and Posamentier, H.W., eds., Tropical Deltas of Southeast Asia—Sedimentology, Stratigraphy, and Petroleum Geology: SEPM, Special Publication 76, p. 147–173.

Dalrymple, R.W., Kurcinka, C.E., Jablonski, B.V.J., Ichaso, A.A., and MacKay, D.A., 2015, Deciphering the relative importance of fluvial and tidal processes in the fluvial-marine transition, *in* Ashworth P.J., Best J.L., and Parsons, D.R., eds., Fluvial-Tidal Sedimentology: Amsterdam, Elsevier, p. 3-40.

Dashtgard, S.E., and La Croix, A.D., 2015. Sedimentological trends across the tidal-fluvial transition, Fraser River, Canada: a review and some broader implications. In: P.J. Ashworth, J.L. Best and D.R. Parsons (Editors), Fluvial-Tidal Sedimentology, Developments in Sedimentology, 68, Elsevier, p. 111-126.

Dashtgard, S.E., MacEachern, J.A., Frey, S.E., and Gingras, M.K., 2012, Tidal effects on the shoreface: towards a conceptual framework: Sedimentary Geology, v. 279, p. 42-61.

Davies, P.J., Bubela, B., and Ferguson, J., 1978, The formation of ooids: Sedimentology, v. 25, p. 703-730.

Davis, R.A., 2012, Tidal signatures and their preservation potential in stratigraphic sequences, *in* Davis R.A. Jr., and Dalrymple, R.W., eds., Principles of Tidal Sedimentology: Berlin, Springer-Verlag, p. 35-55.

Desjardins, P.R., Buatois, L.A., and Mangano, 2012, Tidal Flats and Subtidal Sand Bodies, *in* Knaust, D., and Bromley, R.G., eds., Trace fossils as indicators of sedimentary environment: Elsevier, Developments in Sedimentology, v. 64, p. 529-561

Dunham, R.J., 1962, Classification of carbonate Rocks according to depositional texture, *in* Ham, W.E., ed., Classification of Carbonate Rocks: American Association of Petroleum Geologists, Memoir 1, p. 108-121.

Einsele, G., 2000, Sedimentary Basins: Evolution, Facies, and Sediment Budget: Berlin, Springer-Verlag, 792 p.

Emery, D., and Myers, K.J., 1996, Sequence Stratigraphy: Victoria, Australia, Blackwell Science Ltd., 291 p.

Enay, R., Mangold, C., Alméras, Y., and Hughes G.W., 2009, The Wadi ad Dawasir “delta”, central Saudi Arabia: GeoArabia, v. 14, p. 17-52.

Faqira, M., Rademakers, M., and Afifi, A.M., 2009. New insights into the Hercynian Orogeny, and their implications for the Paleozoic hydrocarbon system in the Arabian Plate: GeoArabia, v. 14, p. 199-228.

Galloway, W.E., 1975, Process framework for describing the morphologic and stratigraphic evolution of deltaic depositional systems, *in* Broussard, M.L., ed., Deltas– Models for exploration: Houston Geological Society, p. 87-98.

Ginsburg R.N., 1975, Tidal Deposits: New York, Springer-Verlag, 428 p.

Golonka, J., 2007, Late Triassic and Early Jurassic palaeogeography of the world: Palaeogeography, Palaeoclimatolology, Palaeoecolology, v. 244, p. 297-307.

Gugliotta, M., Flint, S.S., Hodgson, D.M., and Veiga, G.D., 2016, Recognition criteria, characteristics and implications of the fluvial to marine transition zone in ancient deltaic deposits (Lajas Formation, Argentina): Sedimentology, v. 63, p. 1971–2001.

Gugliotta, M., Saito, Y., Nguyen, V. L., Ta, T. K. O., Nakashima, R., Tamura, T., Uehara, K., Katsuki, K., and Yamamoto, S., 2017, Process regime, salinity, morphological, and sedimentary trends along the fluvial to marine transition zone of the mixed-energy Mekong River Delta, Vietnam, *in* Ogston, A.S., Allison, M.A., Mullarney, J.C., Nittrouer, C.A., eds., Sediment- and Hydro-Dynamics of the Mekong Delta: From Tidal River to Continental Shelf: Continental Shelf Research, v. 147, p. 7–26.

Gugliotta, M., Saito, Y., Nguyen, V.L., Ta, T.K.O., and Tamura, T., 2019, Sediment distribution and depositional processes along the fluvial to marine transition zone of the Mekong River delta, Vietnam: Sedimentology, v. 66, p. 146–164.

Hallam, A., and Bradshaw, M.J., 1979, Bituminous shales and oolitic ironstones as indicators of transgressions and regressions: Geological Society of London, v. 136, p. 157-164.

Haq, B.U., and Al-Qahtani, A.M., 2005, Phanerozoic cycles of sea-level change on the Arabian Platform: GeoArabia, v. 10, p. 127–160.

Haq, B.U., Hardenbol, J., and Vail, P., 1988, Mesozoic and Cenozoic chronostratigraphy and cycles of sea-level change, *in* Wiglus, C.K., Hastings, B. S., Kendall, C.G., Posmentier, H.W., Ross, C.A., and Van Wagoner, J. C., eds., Sea-Level Change: an Integrated Approach :SEPM, v. 42, p. 71–108.

Harms, J.C., Southard, J.B., Spearing, D.R., and Walker, R.G., 1975, Depositional Environments as Interpreted from Primary Sedimentary Structures and Stratification Sequences: SEPM, Short Course 2, 161 p.

Harris, P., Heap, A., Bryce, S., Porter-Smith, R., Ryan, D., and Heggie, D., 2002, Classification of Australian clastic coastal depositional environments based upon a quantitative analysis of wave, tidal, and river power: Journal of Sedimentary Research, v. 72, p. 858-870.

Hein, F.J., 2015, The Cretaceous McMurray oil sands, Alberta, Canada: A world-class, tidally influenced fluvial–estuarine system—An Alberta government perspective, *in* Ashworth P.J., Best J.L., and Parsons, D.R., eds., Fluvial-Tidal Sedimentology: Amsterdam, Elsevier, p. 561-621.

Heldreich, G., Redfern J., Legler B., Gerdes K., and Williams B.P.J., 2017, Challenges in characterizing subsurface paralic reservoir geometries: a detailed case study of the Mungaroo Formation, North West Shelf, Australia, *in* Hampson, G.J., Reynolds, A.D., Kostic, B., and Wells, M.R., eds., Sedimentology of Paralic Reservoirs: Recent Advances: Geological Society of London, Special Publications 444, p. 59–108.

Howell, J.A., Skorstad, A., MacDonald, A., Fordham, A., Flint, S., Fjellvoll, B., and Manzocchi, T., 2008, Sedimentological parameterization of shallow-marine reservoirs: Petroleum Geoscience, v. 14, p. 17-34.

Hubbard, S.M., Smith, D.G., Nielsen, H., Leckie, D.A., Fustic, M., Spencer, R.J., and Bloom, L., 2011, Seismic geomorphology and sedimentology of a tidally influenced river deposit, Lower Cretaceous Athabasca oil sands, Alberta, Canada. American Association of Petroleum Geologists, Bulletin, v. 95, p. 1123-1145.

Jackson, M.D., Yoshida, S., Muggeridge, A.H., and Johnson, H.D. 2005, Three-dimensional reservoir characterisation and flow simulation of heterolithic tidal sandstones: American Association of Petroleum Geologists, Bulletin, v. 89, p. 507–528.

Johnson, H.D., and Baldwin, C.T., 1986., Shallow siliciclastic seas, *in* Reading, H.G., ed., Sedimentary Environments and Facies: London, Blackwell, p. 229-282.

Klein, G.V., 1985, Intertidal flats and intertidal sand bodies, *in* Davis, R.A., ed., Coastal Sedimentary Environments, 2nd Edition: New York, Springer-Verlag, p. 187–224.

La Croix, A., and Dashtgard, S., 2014, Of sand and mud: sedimentological criteria for identifying the turbidity maximum zone in a tidally influenced river: Sedimentology, v. 61, p. 1961–1981.

La Croix, A.D. and Dashtgard, S.E., 2015, A synthesis of depositional trends in intertidal and upper subtidal sediments across the tidal-fluvial transition in the Fraser River, Canada: Journal of Sedimentary Research, v. 85, p. 683-698.

La Croix, A.D., Dashtgard, S.E., and MacEachern, J.A., 2019a, Using a modern analogue to interpret depositional position in ancient fluvial-tidal channels: example from the McMurray Formation, Canada: Geoscience Frontiers, v. 10, p. 2219-2238.

La Croix, A.D., Wang, J., He, J., Hannaford, C., Bianchi, V., Esterle, J.S., and Underschultz, J.R., 2019b, Widespread nearshore and shallow marine deposition within the Lower Jurassic Precipice Sandstone and Evergreen Formation in the Surat Basin, Australia: Marine and Petroleum Geology, v. 109, p. 760-790.

Livera, S.E., and Caline, B., 1990, The sedimentology of the Brent Group in the Cormorant block IV oilfield: Journal of Petroleum Geology, v. 13, p. 367-396.

Loisel, H., Mangin, A., Vantrepotte, V., Dessailly, D., Dinh, D.N., Garnesson, P., Ouillon, S., Lefebvre, J.P., Meriaux, X., and Phan, T.M., 2014. Variability of suspended particulate matter concentration in coastal waters under the Mekong's influence from ocean color (MERIS) remote sensing over the last decade: Remote Sensing of Environment, v. 150, p. 218-230.

MacEachern, J.A., and Bann, K.L., 2008, The role of ichnology in refining shallow marine facies models, *in* Hampson, G., Steel, R., Burgess, P., Dalrymple, R., eds., Recent Advances in Models of Siliciclastic Shallow-Marine Stratigraphy: SEPM, Special Publication 90, p. 73–116.

MacEachern, J.A., Raychaudhuri, I., and Pemberton, S.G., 1992, Stratigraphic applications of the *Glossifungites* ichnofacies: delineating discontinuities in the rock record, *in* Pemberton, S.G., ed., Application of Ichnology to Petroleum Exploration: A Core Workshop: SEPM, p. 169–198.

MacEachern, J.A., Bann, K.L., Pemberton, S.G. and Gingras, M.K., 2007a, The ichnofacies paradigm: high-resolution paleoenvironmental interpretation of the rock record, *in* MacEachern, J.A., Bann, K.L., Gingras, M.K. and Pemberton, S.G., eds., Applied Ichnology: SEPM, p. 27-64.

MacEachern, J.A., Pemberton, S.G., Bann, K.L. and Gingras, M.K., 2007b, Departures from the Archetypal Ichnofacies: Effective Recognition of Physico-Chemical Stresses in the Rock

Record, *in* MacEachern, J.A., Bann, K.L., Gingras, M.K. and Pemberton, S.G., eds., Applied Ichnology: SEPM, p. 65-93.

MacEachern, J.A., Dashtgard, S.E., Knaust, D., Catuneanu, O., Bann, K.L., and Pemberton, S.G., 2012, Sequence stratigraphy, *in* Knaust, D., and Bromley, R.G., eds., Trace Fossils as Indicators of Sedimentary Environments: Developments in Sedimentology, v. 64, p. 157–194.

Martin, C.A.L., 1995, The origin of massive sandstone facies in an ancient braided river deposits [PhD Thesis]: Durham University, Durham, United Kingdom, 329 p.

Martini, I., and Aldinucci M., 2017, Sedimentation and basin-fill history of the Pliocene succession exposed in the northern Siena-Radicofani Basin (Tuscany, Italy): a sequence-stratigraphic approach: Research in Palaeontology and Stratigraphy, v. 123, p. 407-432.

Martinius, A.W., and Gowland, S., 2011, Tide-influenced fluvial bedforms and tidal bore deposits (late Jurassic Lourinhã Formation, Lusitanian Basin, Western Portugal): Sedimentology, v. 58, p. 285-324.

Martinius, A.W., Ringrose P.S., Brostrom , C., Elfenbein, C., Nass, A., and Ringas, J.E., 2005, Reservoir Challenges of Heterolithic Tidal Sandstone Reservoirs in Halten Terrace, mid-Norway: Petroleum Geoscience, v. 11, p. 3-16.

Martinius, A.W., Jablonski, B.V.J., Fustic, M., Strobl, R., and Van den Berg, J.H., 2015, Fluvial to tidal transition zone facies in the McMurray Formation (Christina River, Alberta, Canada), with emphasis on the reflection of flow intensity in bottomset architecture, *in* Ashworth P.J., Best J.L., and Parsons, D.R., eds., Fluvial-Tidal Sedimentology: Amsterdam, Elsevier, v. 68, p. 445–480.

Massart, B.Y.G., Jackson, M.D., Hampson, G.J., and Johnson, H.D., 2016, Effective flow properties of heterolithic, cross-bedded tidal sandstones, part 2: flow simulation: American Association of Petroleum Geologists, Bulletin, v. 100, p. 723–742.

Maynard, J.B., 1983, Geochemistry of Sedimentary Ore Deposits: New York, Springer-Verlag, 305 p.

Meene, J.W.H., Boersma, J.R., and Terwindt, J.H.J., 1996, Sedimentary structures of combined flow deposits from the shoreface-connected ridges along the central Dutch coast: Marine Geology, v. 131, p. 151–175.

Miall, A.D., 1985, Architectural-element analysis: a new method of facies analysis applied to fluvial deposits: Earth-Science Reviews, v. 22, p. 261-308.

Nio, S.D., and Yang, C.S., 1991, Diagnostic attributes of clastic tidal deposits: a review, *in* Smith, D.G., Reinson, G.E., Zaitlin, B.A., and Rahmani, R.A., eds., Clastic Tidal Sedimentology: Canadian Society of Petroleum Geologists, Memoir 16, p. 3-28.

Olariu, C., Steel, R.J., Dalrymple, R.W. and Gingras, M.K., 2012, Tidal dunes versus tidal bars: The sedimentological and architectural characteristics of compound dunes in a tidal seaway, the lower Baronia Sandstone (Lower Eocene), Ager Basin, Spain: Sedimentary Geology, v. 279, p. 134-155.

Pemberton, S.G., and Frey, R.W., 1985, The *Glossifungites* ichnofacies: modern examples from the Georgia coast, *in* Curran, H.A., ed., Biogenic Structures: Their Use in Interpreting Depositional Environments: SEPM, Special Publication 35, p. 237–259.

Pemberton, S.G., Reinson, G.E., and MacEachern, J.A., 1992, Comparative ichnological analysis of late Albian estuarine valley-fill and shelf-shoreface deposits, *in* Pemberton, S.G., ed., Applications of Ichnology to Petroleum Exploration: SEPM, Core Workshop 17, p. 291–317.

Pemberton, S.G., and MacEachern, J.A., 1997, The ichnological signature of storm deposits: the use of trace fossils in event stratigraphy, *in* Brett, C.E., ed., Paleontological Event Horizons: New York, Columbia University Press, p. 73-109.

Pemberton, S.G., Spila, M., Pulham, A.J., Saunders, T., MacEachern, J.A., Robbins, D., and Sinclair, I.K., 2003, Ichnology and sedimentology of shallow marine to marginal marine systems: Ben Nevis & Avalon reservoirs, Jeanne d'Arc Basin: Bulletin of Canadian Petroleum Geology, v. 51, p. 206-211.

Pemberton, S.G., MacEachern, J.A., Dashtgard, S.E., Bann, K.L., Gingras M.K., and Zonneveld J-P., 2012, Shorefaces, *in* Knaust, D., and Bromley, R.G., eds., Trace Fossils as Indicators of Sedimentary Environments: Amsterdam, Elsevier, v. 64, p. 563-603.

Porebsky, S.J., and Steel, R.J., 2006, Deltas and sea-level change: Journal of Sedimentary Research, v. 76, p. 390–403.

Powers, R., Ramirez, L., Redmond, C., and Elberg, E., 1966, Geology of the Arabian Peninsula: Washington, D.C., United States Government Printing Office, 147 p.

Powers, R.W., 1968, Lexique Stratigraphique International: Paris, Centre National de la Recherche Scientifique, p. 73–109.

Prokocki, E.W., Best, J.L., Ashworth, P., Parsons, D.R., Sambrook Smith, G.H., Nicholas, A.P., Simpson, C.J., Wang, H., Sandbach, S., and Keevil, C., 2015, Mid to late Holocene geomorphological and sedimentological evolution of the fluvial–tidal zone: Lower Columbia River, WA/OR, USA, *in* Ashworth P.J., Best J.L., and Parsons, D.R., eds., Fluvial-Tidal Sedimentology: Amsterdam, Elsevier, v. 68, p. 193–226.

Rankey, E.C., and Reeder, S.L., 2012, Tidal sands of the Bahamian archipelago, *in* Davis, R.A., and Dalrymple, R.W., eds., Principles of Tidal Sedimentology: Berlin, Springer-Verlag, p. 537–565.

Reineck, H-E., and Wunderlich, F., 1968., Classification and origin of flaser, and lenticular bedding: Sedimentology, v. 11, 99–104.

Reineck, H-E., and Singh, I.B., 1980, Depositional Sedimentary Environments - With Reference to Terrigenous Clastics, 2nd Edition: Berlin, Springer-Verlag, 549 p.

Reynolds, A.D., 2017, Paralic reservoirs, *in* Hampson, G.J., Reynolds, A.D., Kostic, B., and Wells, M.R., eds., Sedimentology of Paralic Reservoirs: Recent Advances: Geological Society of London, Special Publication 444, p. 7-34.

Ringrose, P.S., Nordhal, K., and Wen, R., 2005, Vertical permeability estimation of heterolithic tidal deltaic sandstones: Petroleum Geoscience, v. 11, p. 29–36.

Robert, C., and Chamley, H., 1991, Development of early Eocene warm climates, as inferred from clay mineral variations in oceanic sediments: Global and Planetary Change, v. 3, p. 315–331.

Schlaich, M., and Aigner, T., 2017, Facies and integrated sequence stratigraphy of an Epeiric Carbonate Ramp Succession: Dhruma Formation, Sultanate of Oman: Sedimentology, v. 3, p. 62-132.

Scotese, C.R., 2001, Atlas of Earth History, Vol. 1, Palaeogeography , 52 p., Paleomap Project, Arlington, Texas.

Seton, M., Muller, R.D., Zahirovi c, S., Gaina, C., Torsvik, T., Shephard, G., Talsma, A., Gurnis, M., Turner, M., Maus, S., and Chandler, M., 2012, Global continental and ocean basin reconstructions since 200 Ma: Earth-Science Review, v. 113, p. 212–270.

Shchepetkina, A., Gingras, M.K., and Pemberton, S.G., 2016, Sedimentology and ichnology of the fluvial reach to inner estuary of the Ogeechee River estuary, Georgia, USA: Sedimentary Geology, v. 342, p. 202–217.

Shiers, M.N., Mountney, N.P., Hodgson, D.M., and Cobain, S.L., 2014, Depositional Controls on Tidally Influenced Fluvial Successions, Neslen Formation, Utah, USA: Sedimentary Geology, v. 311, p. 1-16.

Soliman, F.A., and Al-Shamlan, A.A., 1982, Review on the geology of the Cretaceous sediments of the Rub' al-Khali, Saudi Arabia: Cretaceous Research, v. 3, p. 187–194.

Stampfli, G.M., and Borel, G.D., 2002, A plate tectonic model for the Paleozoic and Mesozoic constrained by dynamic plate boundaries and restored synthetic oceanic isochrons: Earth and Planetary Science Letters, v. 196, p. 17–33.

Stewart, S.A., 2016, Structural geology of the Rub' Al-Khali Basin, Saudi Arabia: Tectonics, v. 35, p. 2417–2438.

Stewart, S.A., Reid, C.T., Hooker, N.P., and Kharouf, O.W., 2016, Mesozoic siliciclastic reservoirs and petroleum system in the Rub' Al-Khali basin, Saudi Arabia: American Association of Petroleum Geologists, Bulletin, v. 100, p. 819–841.

Tawfik, M., Al-Dabbagh, M., and El-Sorogy, A., 2016, Sequence stratigraphy of the late middle Jurassic open shelf platform of the Tuwaiq Mountain Limestone Formation, central Saudi Arabia: Proceedings of the Geologists' Association, v. 127, p. 395–412.

Taylor, A.M. and Goldring, R., 1993, Description and analysis of bioturbation and ichnofabric: Geological Society of London, v. 150, p. 141-148.

Thomas, R.G., Smith, D.G., Wood, J.M., Visser, J., Calverley-Range, E.A., and Koster, E.H., 1987, Inclined heterolithic stratification - terminology, description, interpretation and significance: Sedimentary Geology, v. 53, p. 123-179.

Tirsgaard, H., 1996, Cyclic sedimentation of carbonate and siliciclastic deposits on a late Precambrian ramp: the Elisabeth Bjerg Formation (Eleonore Bay Supergroup), East Greenland: Journal of Sedimentary Research, v. 66, p. 699-712.

Vakarelov, B.K., and Ainsworth, R.B., 2013, A hierarchical approach to architectural classification in marginal-marine systems: bridging the gap between sedimentology and sequence stratigraphy: American Association of Petroleum Geologists, Bulletin, v. 97, p .1121-1161.

Van de Lageweg, W.I., Braat, L., Parsons, D.R., and Kleinhans, M. G., 2018, Controls on mud distribution and architecture along the fluvial-to-marine transition: Geology, v. 46, p. 971– 974.

Van den Berg, J.H., Boersma, J.R., and Van Gelder, A., 2007, Diagnostic sedimentary structures of the fluvial–tidal transition zone. Evidence from deposits of the Rhine Delta: Netherland Journal of Geoscience, v. 86, p. 253–272.

Van Houten, F.B., 1985, Oolitic ironstones and contrasting Ordovician and Jurassic paleogeography: Geology, v. 13, p. 722-24.

Van Wagoner, J.C., Mitchum, R.M., Campion, K.M., and Rahmanian, V.D., 1990, Siliciclastic Sequence Stratigraphy in Well Logs, Cores and Outcrops: Concepts for High-resolution Correlation of Time and Facies: American Association of Petroleum Geologists, Methods in Exploration Series 7, 55 p.

Vaslet, D., Manivit, J., Le Nindre, Y., Brosse, J., Fourniguet, J., and Delfour, J., 1983, Explanatory Notes to the Geologic Map of the Wadi Ar Rayn Quadrangle, Kingdom of Saudi Arabia: Saudi Arabian Deputy Ministry for Mineral Resources, Geoscience Map GM-63C.

Vicalvi, M.A., and Milliman, J.D., 1977, Calcium carbonate sedimentation on continental shelf off Southern Brazil, with special reference to Benthic Foraminifera, *in* Frost, S.H., Weiss, M.P., and Saunders, J.B., eds., Reefs and Related Carbonates–Ecology and Sedimentology: American Association of Petroleum Geologists, Studies in Geology 4, p. 313-328.

Visser, M.J., 1980, Neap-spring cycles reflected in Holocene subtidal large scale bedform deposits: a preliminary note: Geology, v. 8, p. 543-546.

Weaver, C.E., 1989, Clays, Muds, and Shales: Amsterdam, Elsevier, Development in Sedimentology, v. 44, 818 p.

Wightman, D.M., and Pemberton, S.G., 1997, The lower Cretaceous (Aptian) McMurray Formation: an overview of the Fort McMurray area, northeastern Alberta, *in* Pemberton, S.G., and James, D.P., ed., Petroleum Geology of the Cretaceous Mannville Group: Canadian Society of Petroleum Geologists, Memoir 18, p. 312–344.

Ziegler, M.A., 2001, Late Permian to Holocene paleofacies evolution of the Arabian Plate and its hydrocarbon occurrences: GeoArabia, v. 6, p. 445–504.

TABLE CAPTIONS

Table 1. Summary of lithofacies observed in the lower Dhruma Formation.

Table 2. Summary of the facies associations defined in this study, along with their occurrence with respect to well locations.

FIGURE CAPTIONS

Figure 1. A) Simplified regional geological map of the Arabian Peninsula, adapted from Stewart et al. (2016). B) Well distribution map in the study area. The exact geographic location of the wells cannot be published due to the proprietary nature of the dataset. C) Generalized stratigraphy of Eastern Saudi Arabia.

Figure 2. Representative sedimentary logs depicting the different facies associations defined in the lower Dhruma Formation and their vertical relationships. A) "Fluvial channels" and "intertidal flats and pedogenically modified supratidal or floodplain" facies associations. B) "River-influenced tidal bars" facies associations. C) "Weakly storm-affected shoreface and offshore transition zone" and "fluvial-influenced storm-dominated delta-front and prodelta" facies associations; note the occurrence of the oolitic ironstone facies association FA5 below the shoreface successions. D) Carbonate shelf facies associations occurring in the uppermost part of the cored section. E) Simplified paleogeographic map of the lower unit of the lower Dhruma Formation based on this study. F) Legend with color codes for facies associations and symbols used in the sedimentary logs. See text for further explanation.

Figure 3. Representative core photographs of "fluvial channel" facies association (FA1). A,B) massive to faintly bedded sandstone with lag sediments at the bottom and common floating coal debris and mud chips. B) Alternating sandstone and heterolithic facies. D,E) transition between sandstone and heterolithic facies (white arrows indicate double mud drapes in Part D. F) Non-stratified facies of FA2b overlying the FA1. G,H) Thin sections representing the petrography of the sandstone facies (G) and heterolithic facies (H) defined in FA1; note variation in grain size and mud content.

Figure 4. Representative core photographs of " tidal flat" (FA2a, A-C) and "paleosol" (FA2b, D-G) facies associations. A,B) Heterolithic sand and mud facies; note the stacked bidirectional ripple forms (black arrows) and double mud drapes (white arrows). C) Intense bioturbation in the sand-mud alternation; D, E) Kaolinite-rich sandstone, siltstone, and mudstone with intense rooting; note the color mottling in photograph E. F, G) Coaly mudstone. H, I) representative thin sections of the heterolithic facies of FA2a.

Figure 5. Representative core photographs of the "fluvial-influenced tidal bars" facies association (FA3). A) Cross-bedded sandstone with apparent bundled bedsets showing internal mud drapes. B, C) Cross-stratified sandstone showing thin beds of very coarse sand in medium-grained sandstone; note the double mud drapes in part B. D, E) Heterolithic and kaolinite-rich deposits that overlie the tidal-bar deposits. F, G) Representative thin sections of tidal-bar facies; note the presence of kaolinite.

Figure 6. Representative core photographs of "offshore-transition zone to shoreface" (FA4a; A-D) and prodelta to delta-front (FA4b; E-I) facies associations. A) Heterolithic facies overlying bioturbated sandstone. B) Slightly asymmetrical wave ripple. C) Bioturbated sandstone. D) Representative thin section showing deformed chamosite ooids in heterolithic facies. E, F) Thin sandstone intervals interbedded with heterolithic and mudstone facies. G, H) Hummocky cross stratification. I) Thin section showing abundant chlorite cement in hummocky cross-stratified sandstone.

Figure 7. Representative core photographs of "open-marine shelf carbonate" facies association (FA5). A, B) Bioturbated limestone. C) Calcareous mudstone. D) Calcareous sandstone overlying massive mudstone. E) Ooid-rich ironstone. F, G) Representative thin-section examples showing calcareous sandstone (F) and ooid-rich ironstone (G).

Figure 8. Rose diagrams showing the dominant dip direction of cross-stratification in different sandstone units, based on analysis of image logs. See Figure 4 for keys to facies associations and symbols.

Figure 9. Cross plots showing thickness and lateral dip extent for analog sedimentary units that broadly match with the defined facies associations, as derived from a sedimentological database (Colombera et al., 2016a). A) Data relating to parasequence-scale sedimentary units representing the product of regression of shoreface and more generally shallow-marine (i.e., encompassing sand-prone offshore transition) sand belts (Colombera et al., 2016a, 2016b; Colombera and Mountney, 2020a). B) Data relating to architectural elements classified as "tidal bar" and "tidal flat".

Figure 10A. Strike-oriented stratigraphic cross section (A-A') showing the distribution of facies associations and key stratigraphic surfaces as correlated along strike in a seaward position.

Figure 10B. Strike-oriented stratigraphic cross section (B-B') showing facies associations and stratigraphic surfaces as correlated along strike in a landward position compared to cross-section A-A'.

Figure 10C. Dip-oriented stratigraphic cross-section (C-C') intersecting the two strike-oriented cross sections (A-A' and B-B') showing the distribution of facies associations and key stratigraphic surfaces as correlated along depositional dip, and documenting the increase in marine deposits towards the northeast (basinward).

Figure 11. A depositional model depicting the evolution of the Middle Jurassic lower Dhruma Formation over five intervals. Each interval represents a synthesis of the five intervals highlighted in Figure 10C.

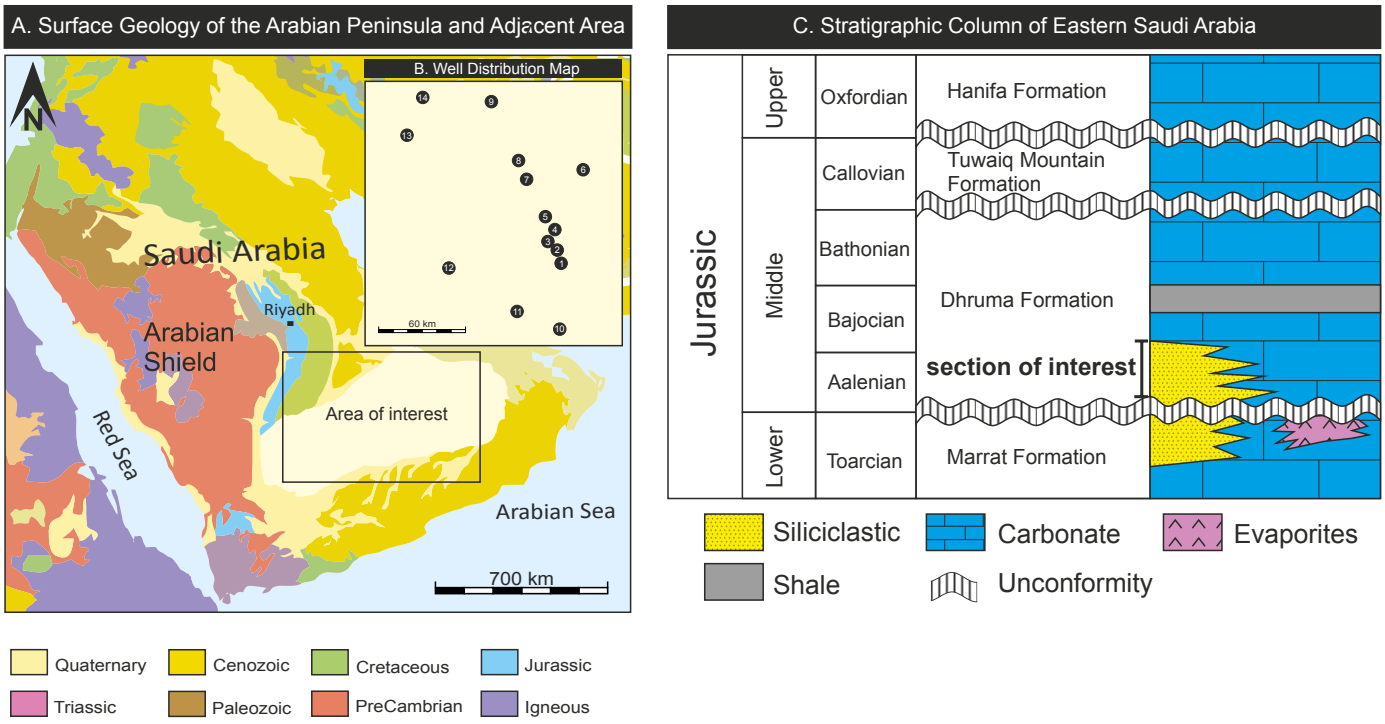
A. Surface Geology of the Arabian Peninsula and Adjacent Area
B. Well Distribution Map
C. Stratigraphic Column of Eastern Saudi Arabia
N
Saudi Arabia
Riyadh
Arabian Shield
Area of interest
Red Sea
Arabian Sea
700 km
60 km
Quaternary
Cenozoic
Cretaceous
Jurassic
Triassic
Paleozoic
PreCambrian
Igneous
Jurassic
Upper
Middle
Lower
Oxfordian
Callovian
Bathonian
Bajocian
Aalenian
Toarcian
Hanifa Formation
Tuwaiq Mountain Formation
Dhruma Formation
section of interest
Marrat Formation
Siliciclastic
Carbonate
Evaporites
Shale
Unconformity

Figure 1

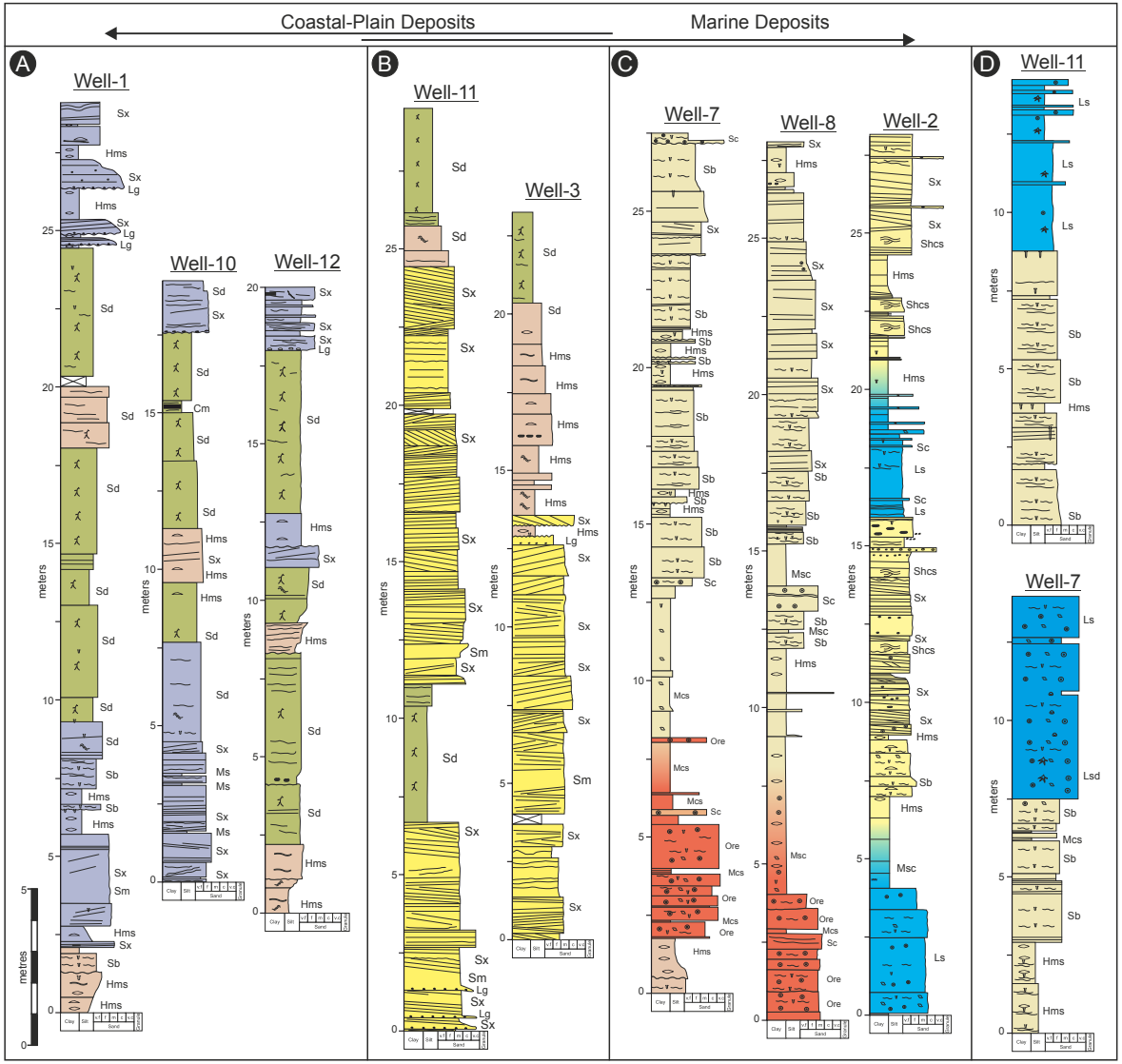

E. Palaeogeographic Map of the Study Area with Well Locations

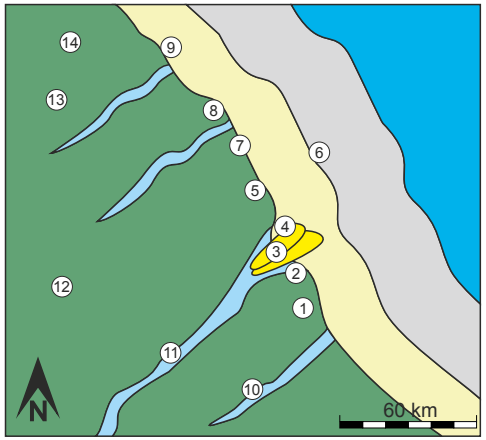

F. Legend

Key to Facies Association

- Fluvial Channel and Overbank (FA1)
- Intertidal Flat (FA2.a)
- Supratidal Flat/Floodplain (Palaeosol) (FA2.b)
- Fluvially influenced Tidal Bars (FA3)
- Weakly Storm-affected Shoreface (FA4.a)
- Storm-Dominated Delta Front (FA4.b)
- Carbonate Shelf (FA5.a)
- Ooid-rich Ironstone (FA5.b)

Key to Sedimentary Structures and Composition

- Cross Bedding
- Irregular Lamination
- Flaser Bedding
- Wavy Bedding
- Lenticular Bedding
- Hummocky Cross-Stratification
- Soft-Sediment Deformation
- Rootlets
- Lag Deposits
- Echinoderms
- Bioturbation
- Coated Grains
- Ooids
- Skeletal Fragments
- Organic and Coal Debris
- Foraminifera

See **Table 1** for facies definition and description

Figure 2

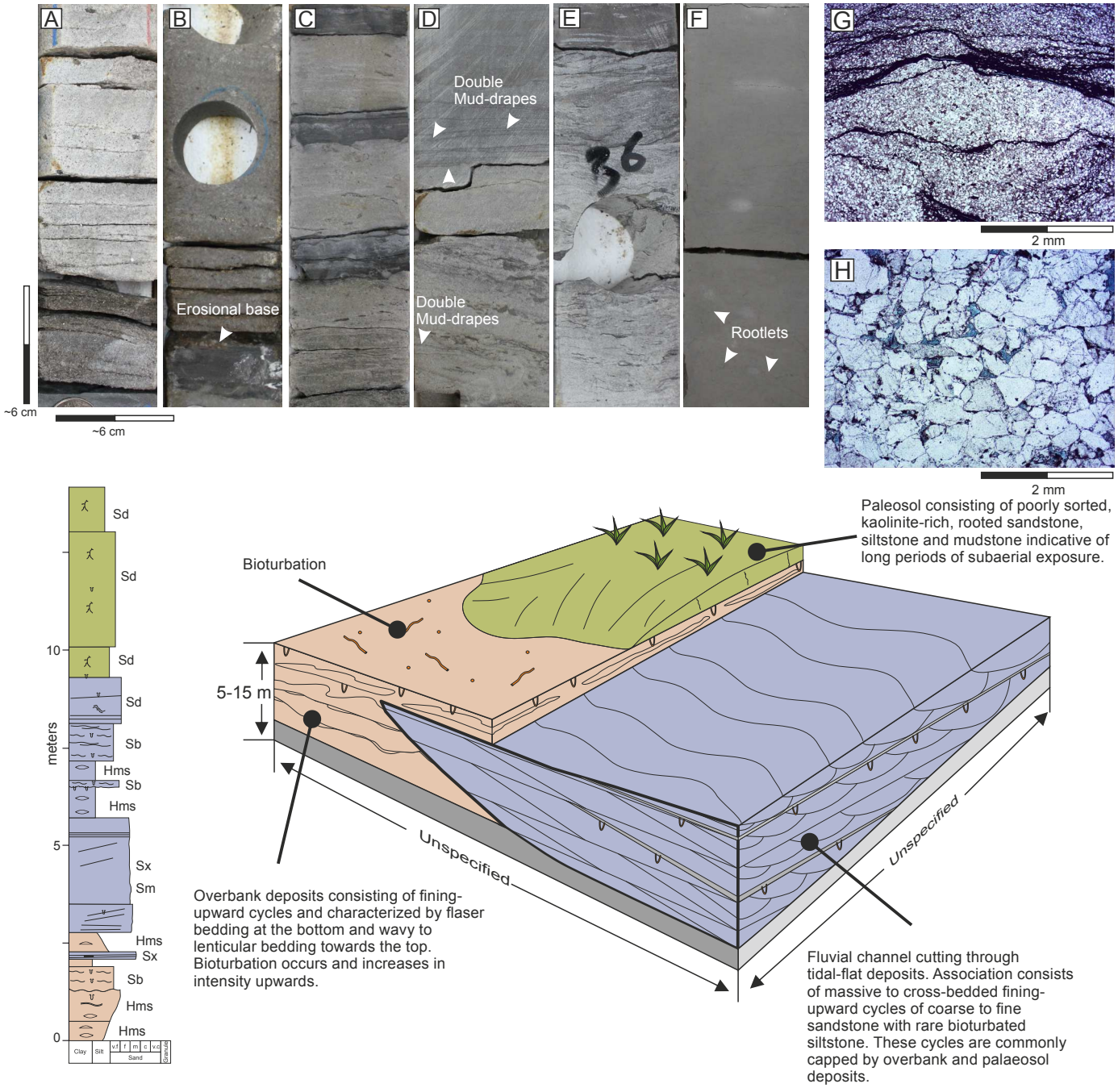
A
B
C
D
E
F
G
H
Double
Mud-drapes
Erosional base
Double
Mud-drapes
Rootlets
36
~6 cm
~6 cm
2 mm
2 mm
Paleosol consisting of poorly sorted, kaolinite-rich, rooted sandstone, siltstone and mudstone indicative of long periods of subaerial exposure.
Bioturbation
5-15 m
Unspecified
Unspecified
Overbank deposits consisting of fining-upward cycles and characterized by flaser bedding at the bottom and wavy to lenticular bedding towards the top. Bioturbation occurs and increases in intensity upwards.
Fluvial channel cutting through tidal-flat deposits. Association consists of massive to cross-bedded fining-upward cycles of coarse to fine sandstone with rare bioturbated siltstone. These cycles are commonly capped by overbank and palaeosol deposits.
meters
10
5
0
Sd
Sd
Sd
Sd
Sb
Hms
Sb
Hms
Sx
Sm
Hms
Sx
Sb
Hms
Hms
Clay
Silt
Sand
vf
f
m
c
v.c
Granule

Figure 3

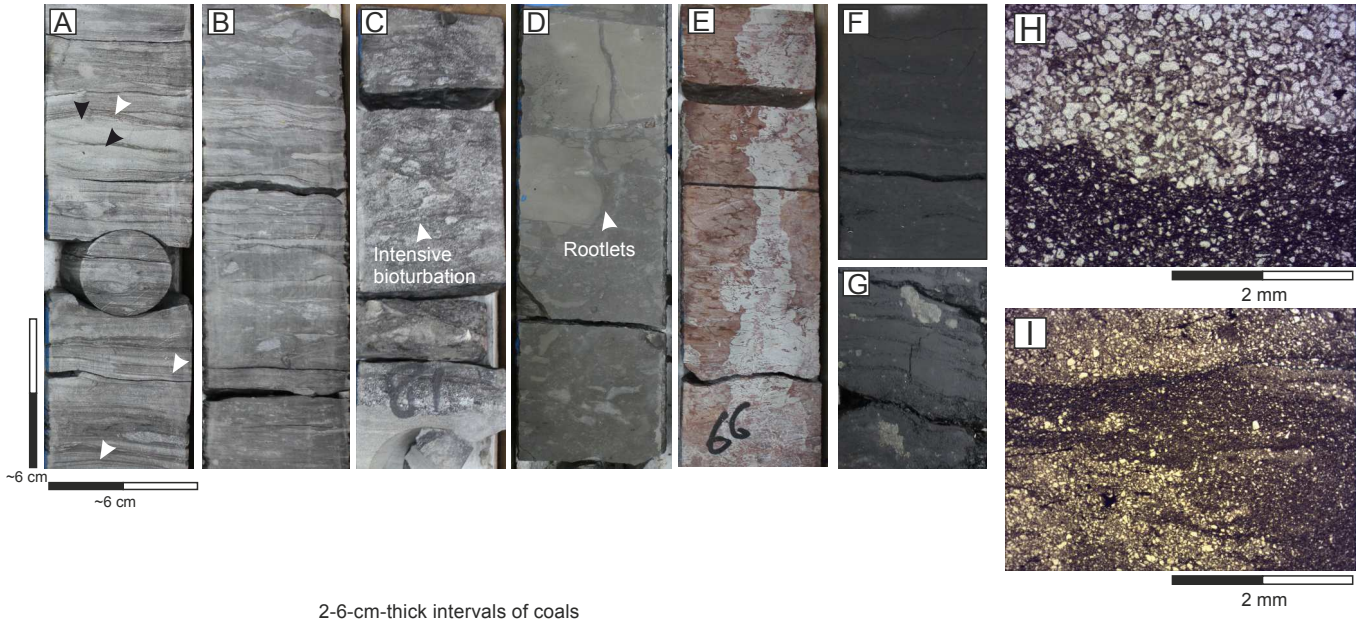
A
B
C
D
E
F
G
H
I
Intensive bioturbation
Rootlets
~6 cm
~6 cm
2 mm
2 mm

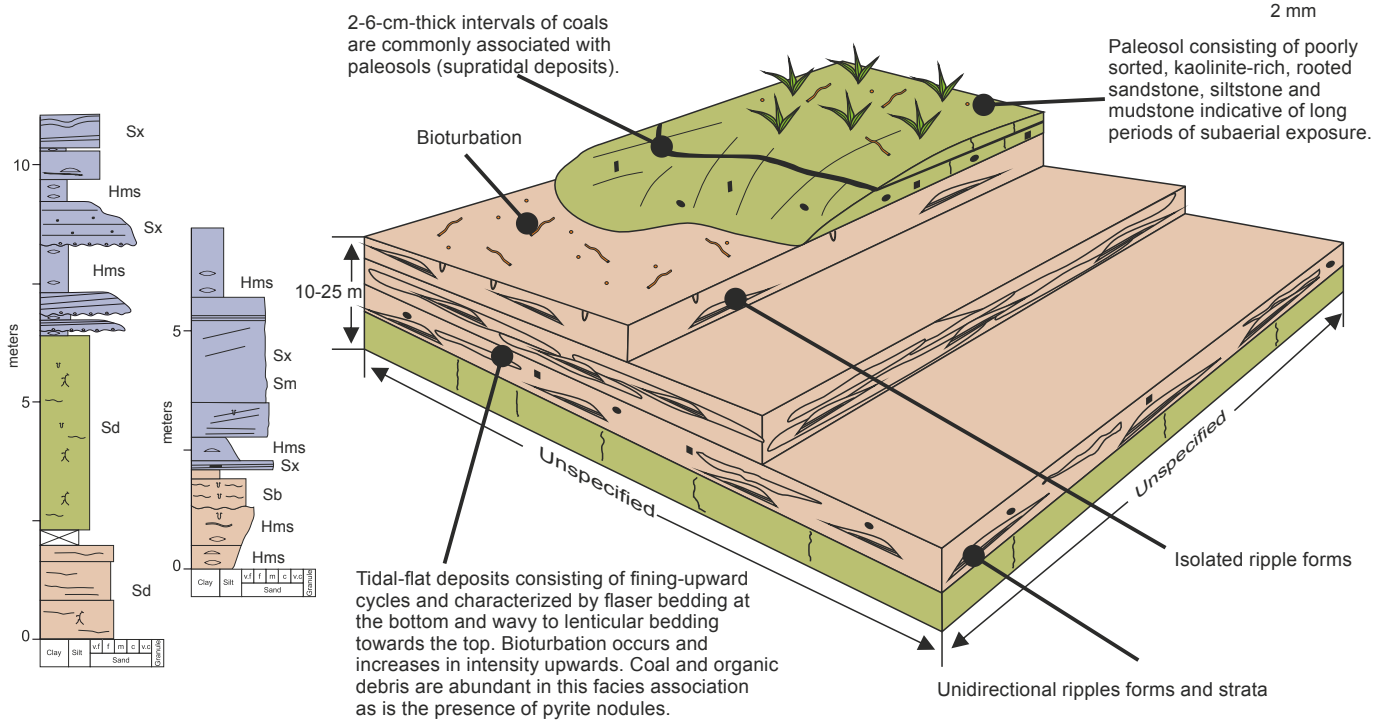
2-6-cm-thick intervals of coals are commonly associated with paleosols (supratidal deposits).
Paleosol consisting of poorly sorted, kaolinite-rich, rooted sandstone, siltstone and mudstone indicative of long periods of subaerial exposure.
Bioturbation
10-25 m
meters
Sx
Hms
Sd
Sm
Sb
Clay
Silt
Sand
Unspecified
Unspecified
Isolated ripple forms
Tidal-flat deposits consisting of fining-upward cycles and characterized by flaser bedding at the bottom and wavy to lenticular bedding towards the top. Bioturbation occurs and increases in intensity upwards. Coal and organic debris are abundant in this facies association as is the presence of pyrite nodules.
Unidirectional ripples forms and strata

Figure 4

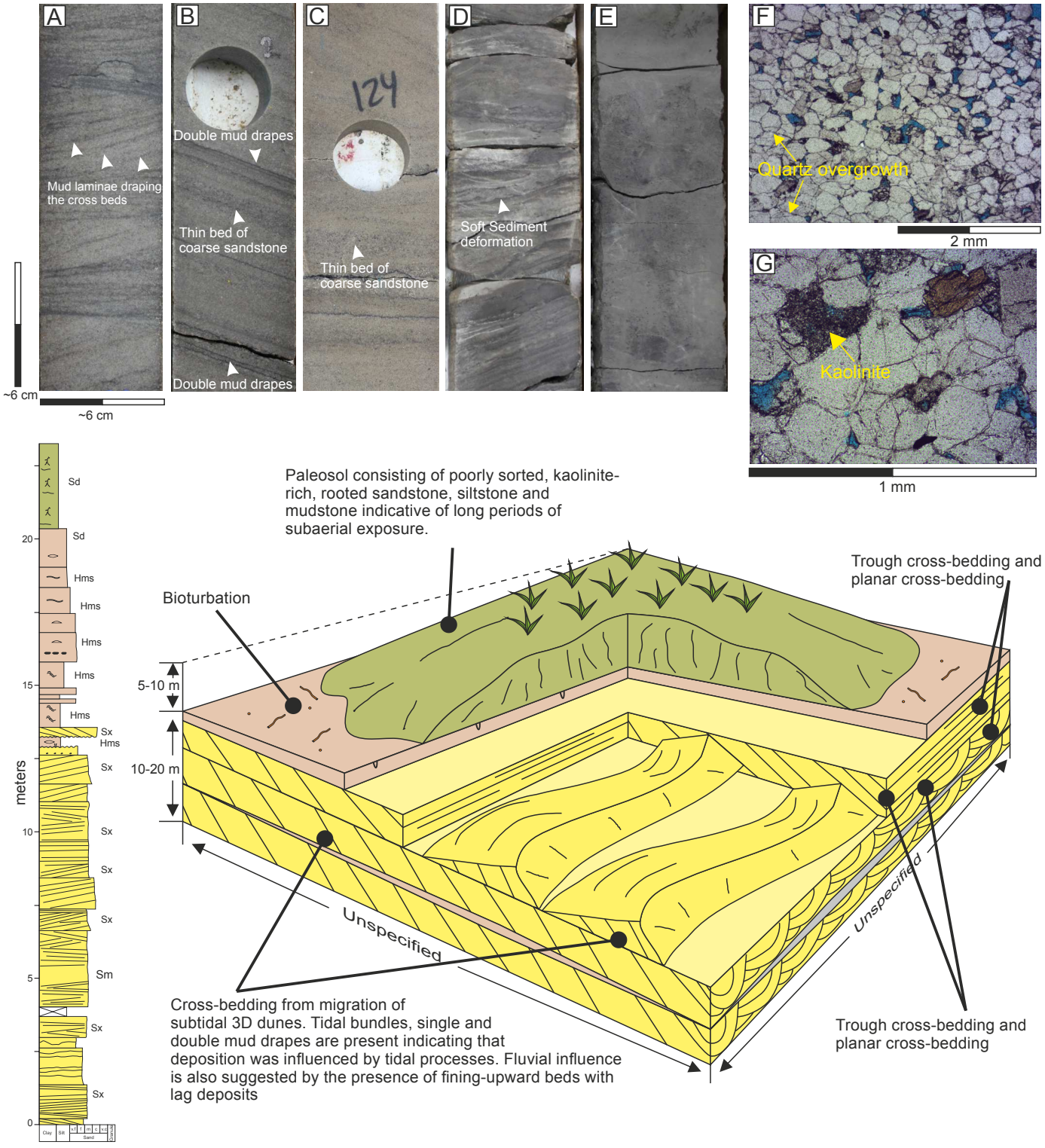
A
B
C
D
E
F
G
Mud laminae draping the cross beds
Double mud drapes
Thin bed of coarse sandstone
Double mud drapes
Thin bed of coarse sandstone
Soft Sediment deformation
Quartz overgrowth
2 mm
Kaolinite
1 mm
~6 cm
~6 cm
meters
Sd
Sd
Hms
Hms
Hms
Hms
Hms
Sx
Hms
Sx
Sx
Sx
Sx
Sm
Sx
Sx
Paleosol consisting of poorly sorted, kaolinite-rich, rooted sandstone, siltstone and mudstone indicative of long periods of subaerial exposure.
Bioturbation
Trough cross-bedding and planar cross-bedding
5-10 m
10-20 m
Unspecified
Unspecified
Cross-bedding from migration of subtidal 3D dunes. Tidal bundles, single and double mud drapes are present indicating that deposition was influenced by tidal processes. Fluvial influence is also suggested by the presence of fining-upward beds with lag deposits
Trough cross-bedding and planar cross-bedding

Figure 5

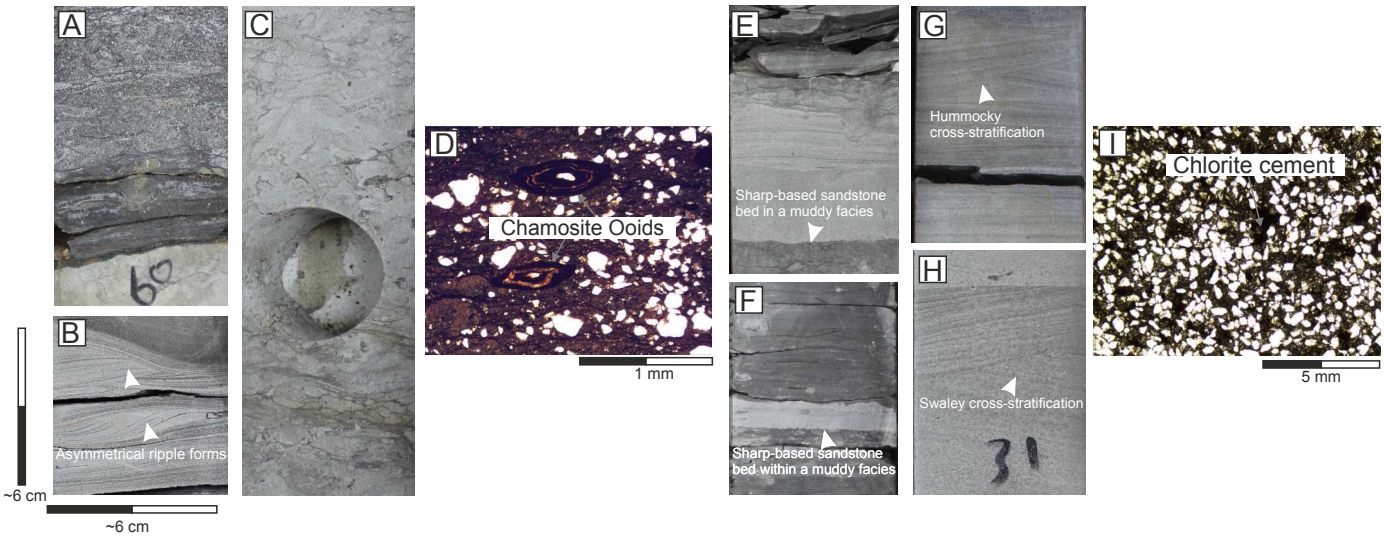
A
B
C
D
Chamosite Ooids
1 mm
E
Sharp-based sandstone bed in a muddy facies
F
Sharp-based sandstone bed within a muddy facies
G
Hummocky cross-stratification
H
Swaley cross-stratification
I
Chlorite cement
5 mm
Asymmetrical ripple forms
~6 cm
~6 cm

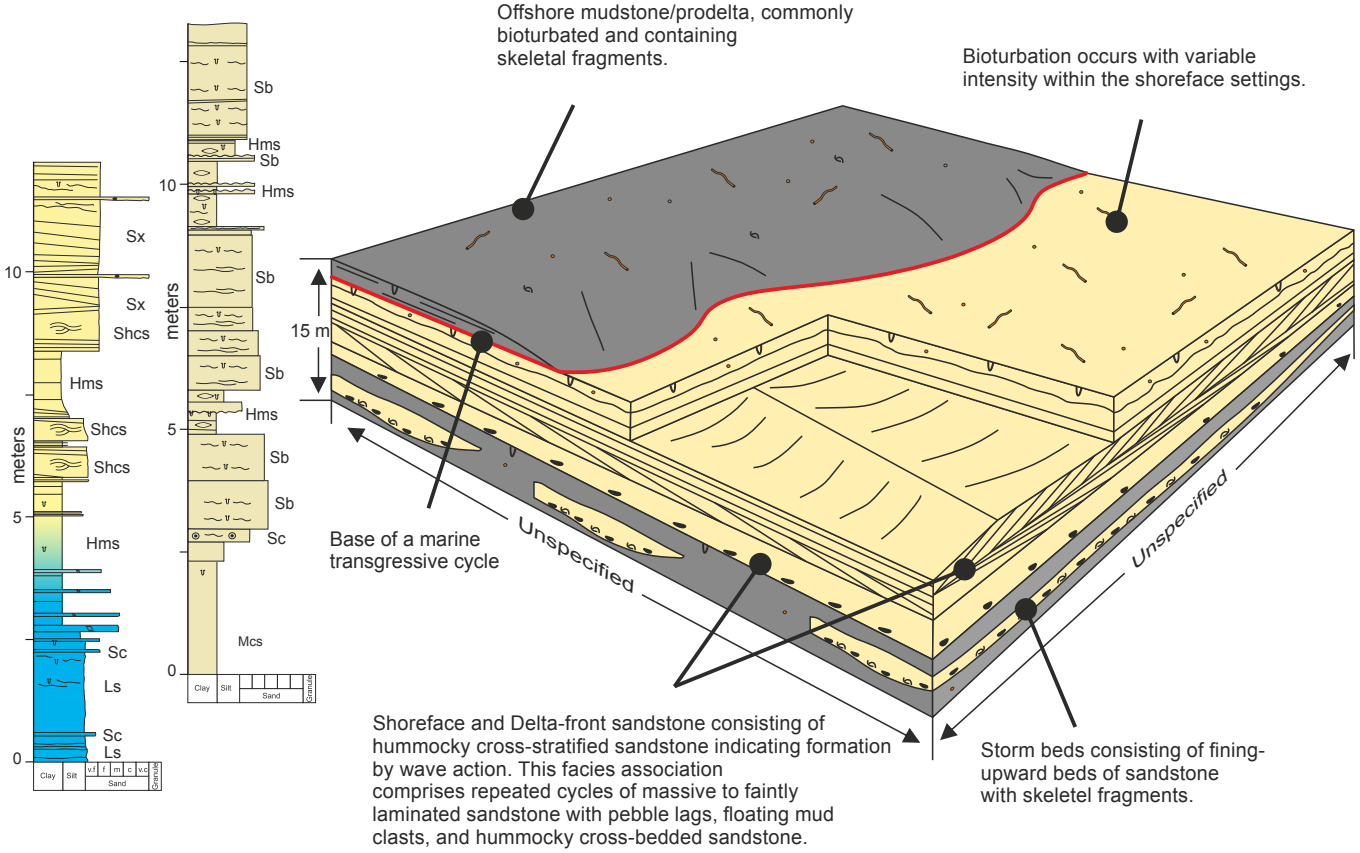
Offshore mudstone/prodelta, commonly bioturbated and containing skeletal fragments.
Bioturbation occurs with variable intensity within the shoreface settings.
meters
Sx
Sx
Shcs
Hms
Shcs
Shcs
Hms
Sc
Ls
Sc
Ls
Sb
Hms
Sb
Hms
Sb
Sb
Hms
Sb
Sb
Sc
Mcs
15 m
Base of a marine transgressive cycle
Unspecified
Unspecified
Shoreface and Delta-front sandstone consisting of hummocky cross-stratified sandstone indicating formation by wave action. This facies association comprises repeated cycles of massive to faintly laminated sandstone with pebble lags, floating mud clasts, and hummocky cross-bedded sandstone.
Storm beds consisting of fining-upward beds of sandstone with skeletel fragments.

Figure 6

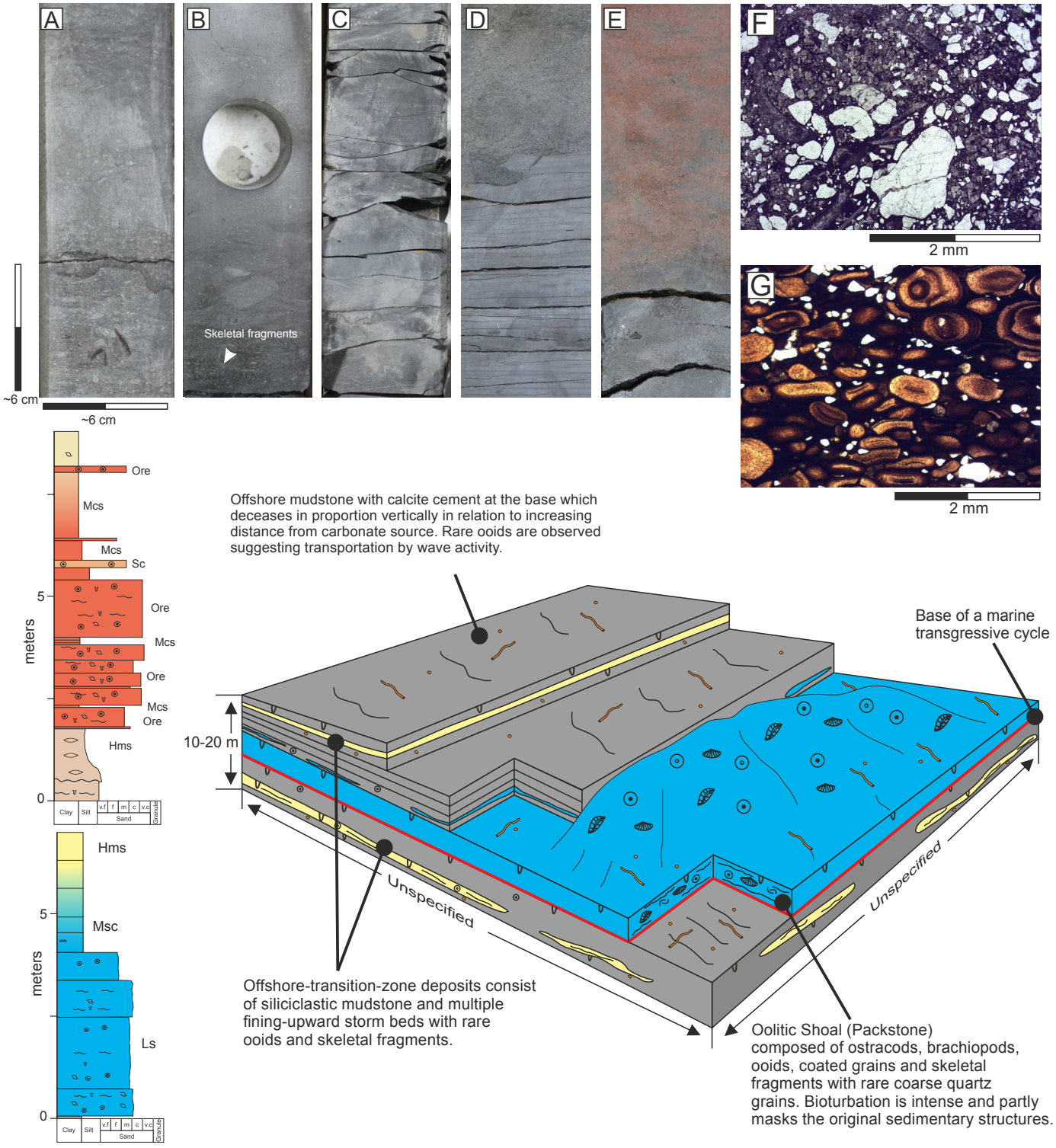
A
B
C
D
E
F
G
Skeletal fragments
~6 cm
~6 cm
2 mm
2 mm
Ore
Mcs
Mcs
Sc
Ore
Mcs
Ore
Mcs
Ore
Hms
meters
5
0
Clay
Silt
v.f
f
m
c
v.c
Granule
Sand
Hms
Msc
Ls
meters
5
0
Offshore mudstone with calcite cement at the base which deceases in proportion vertically in relation to increasing distance from carbonate source. Rare ooids are observed suggesting transportation by wave activity.
10-20 m
Base of a marine transgressive cycle
Unspecified
Unspecified
Offshore-transition-zone deposits consist of siliciclastic mudstone and multiple fining-upward storm beds with rare ooids and skeletal fragments.
Oolitic Shoal (Packstone) composed of ostracods, brachiopods, ooids, coated grains and skeletal fragments with rare coarse quartz grains. Bioturbation is intense and partly masks the original sedimentary structures.

Figure 7

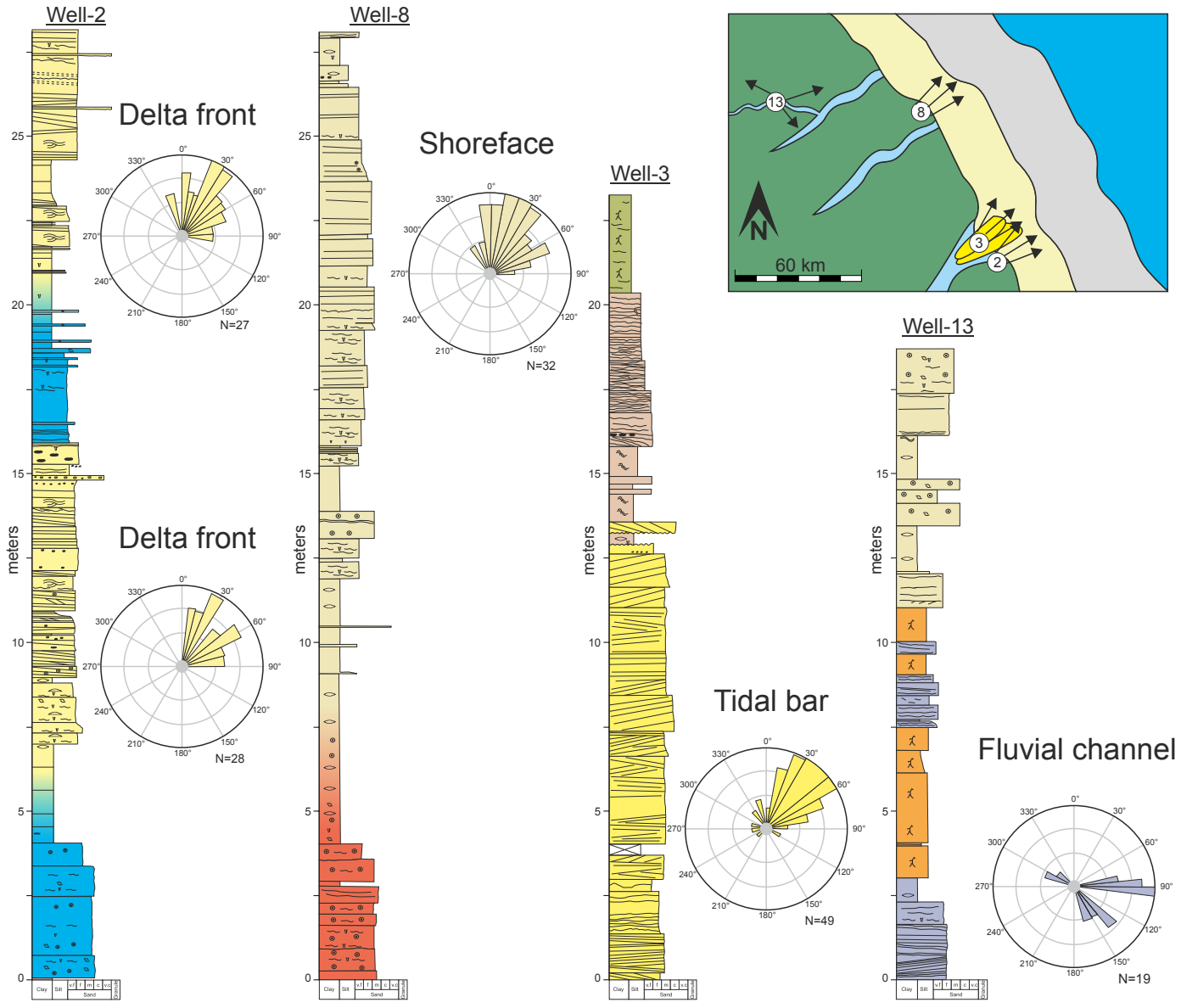
Well-2
Well-8
Well-3
Well-13
Delta front
Delta front
Shoreface
Tidal bar
Fluvial channel
N=27
N=28
N=32
N=49
N=19
meters
60 km
N
13
8
3
2

Figure 8

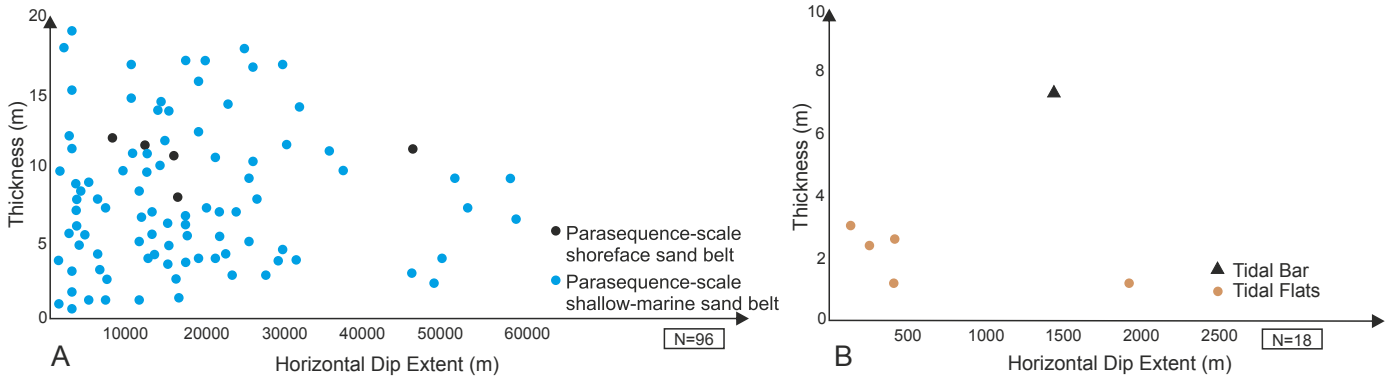
20
15
10
5
0
Thickness (m)
10000
20000
30000
40000
50000
60000
Horizontal Dip Extent (m)
Parasequence-scale shoreface sand belt
Parasequence-scale shallow-marine sand belt
N=96
A
10
8
6
4
2
0
Thickness (m)
500
1000
1500
2000
2500
Horizontal Dip Extent (m)
Tidal Bar
Tidal Flats
N=18
B

Figure 9

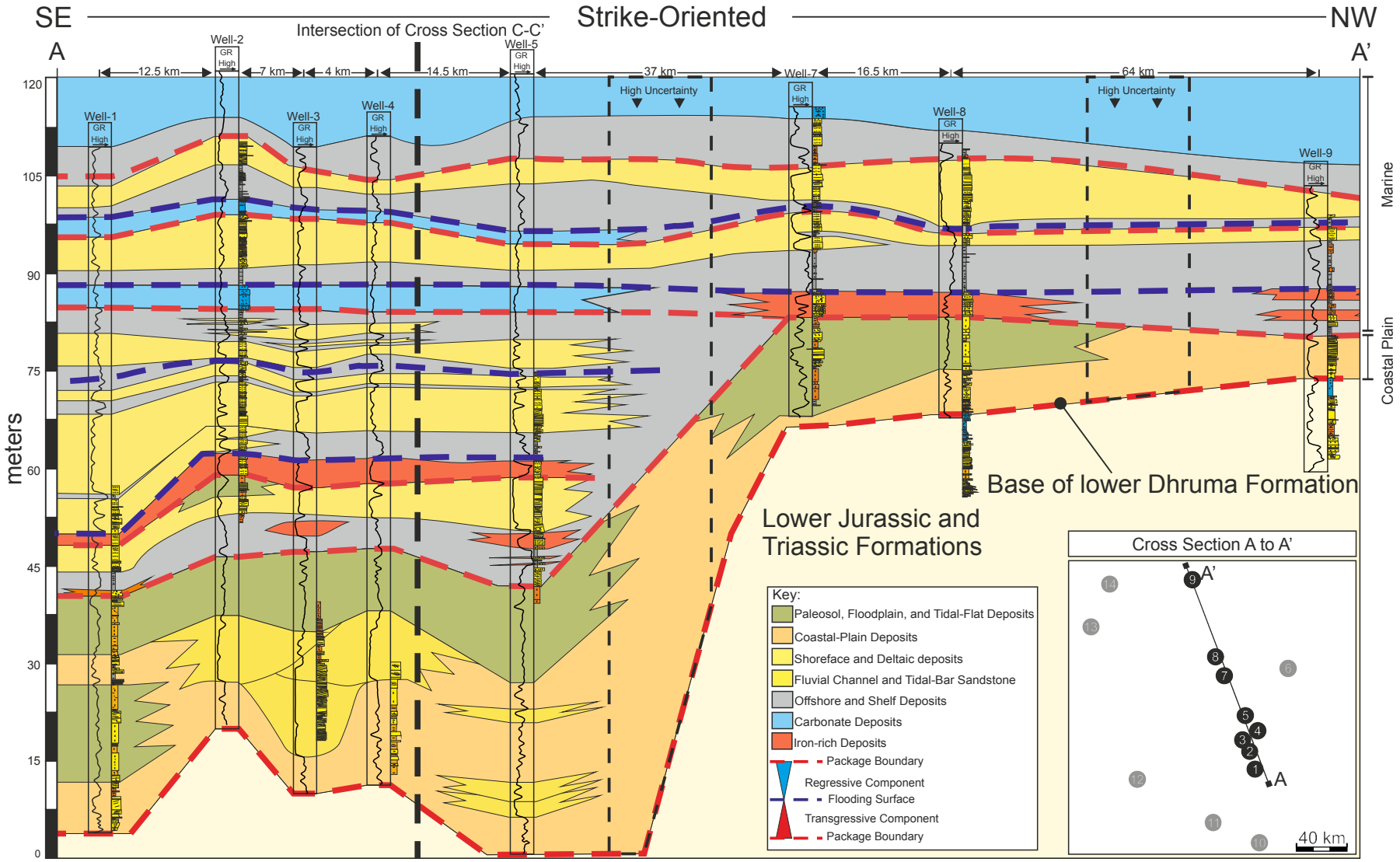
SE
A
Strike-Oriented
NW
A'
Intersection of Cross Section C-C'
Well-1
Well-2
Well-3
Well-4
Well-5
Well-7
Well-8
Well-9
GR
High
12.5 km
7 km
4 km
14.5 km
37 km
16.5 km
64 km
High Uncertainty
High Uncertainty
120
105
90
75
60
45
30
15
0
meters
Marine
Coastal Plain
Base of lower Dhruma Formation
Lower Jurassic and
Triassic Formations
Key:
Paleosol, Floodplain, and Tidal-Flat Deposits
Coastal-Plain Deposits
Shoreface and Deltaic deposits
Fluvial Channel and Tidal-Bar Sandstone
Offshore and Shelf Deposits
Carbonate Deposits
Iron-rich Deposits
Package Boundary
Regressive Component
Flooding Surface
Transgressive Component
Package Boundary
Cross Section A to A'
A'
A
40 km

Figure 10A

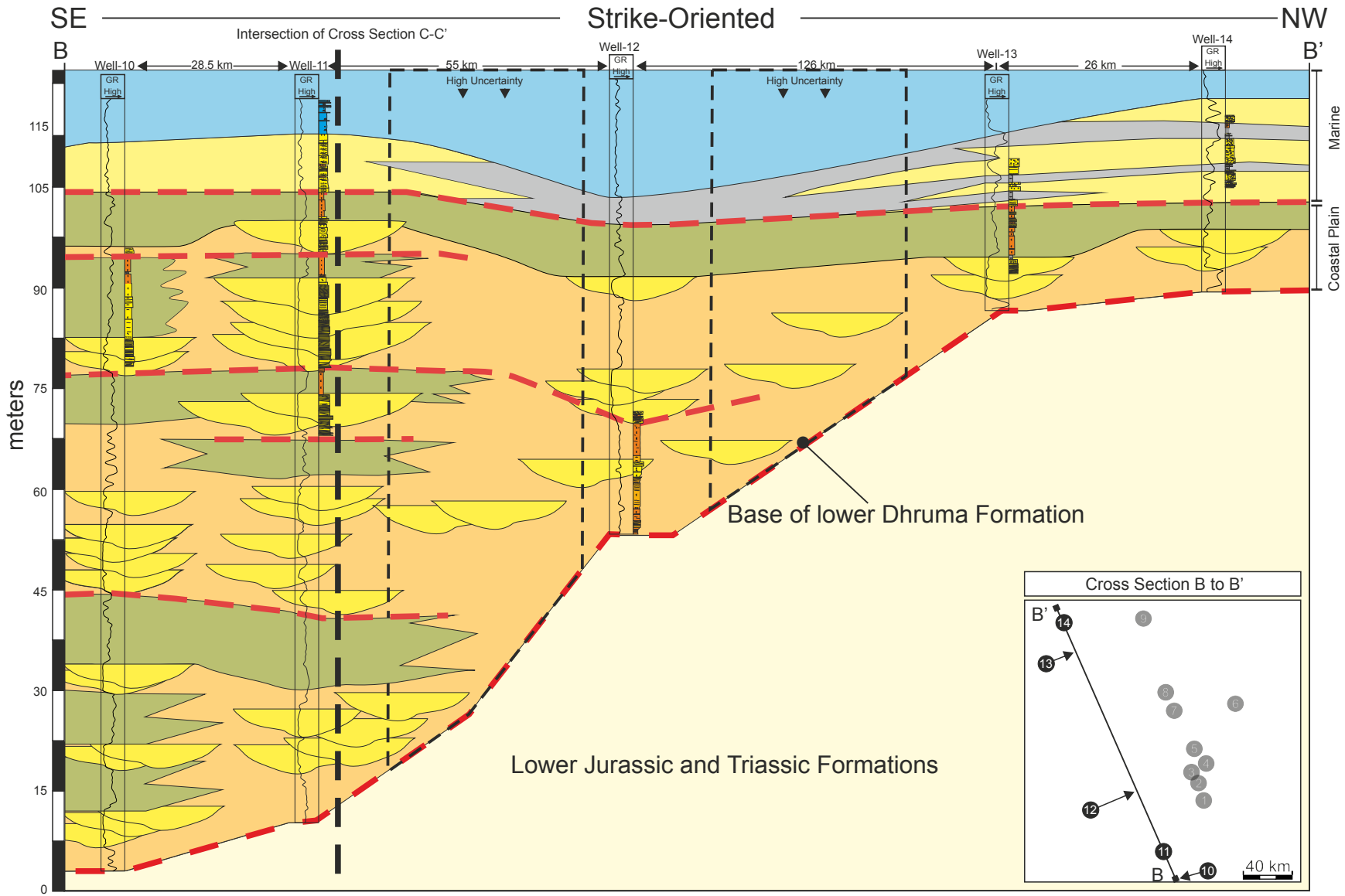
SE
Strike-Oriented
NW
B
B'
Intersection of Cross Section C-C'
Well-10
28.5 km
Well-11
55 km
Well-12
126 km
Well-13
26 km
Well-14
GR
High
High Uncertainty
meters
115
105
90
75
60
45
30
15
0
Marine
Coastal Plain
Base of lower Dhruma Formation
Lower Jurassic and Triassic Formations
Cross Section B to B'
40 km

Figure 10B

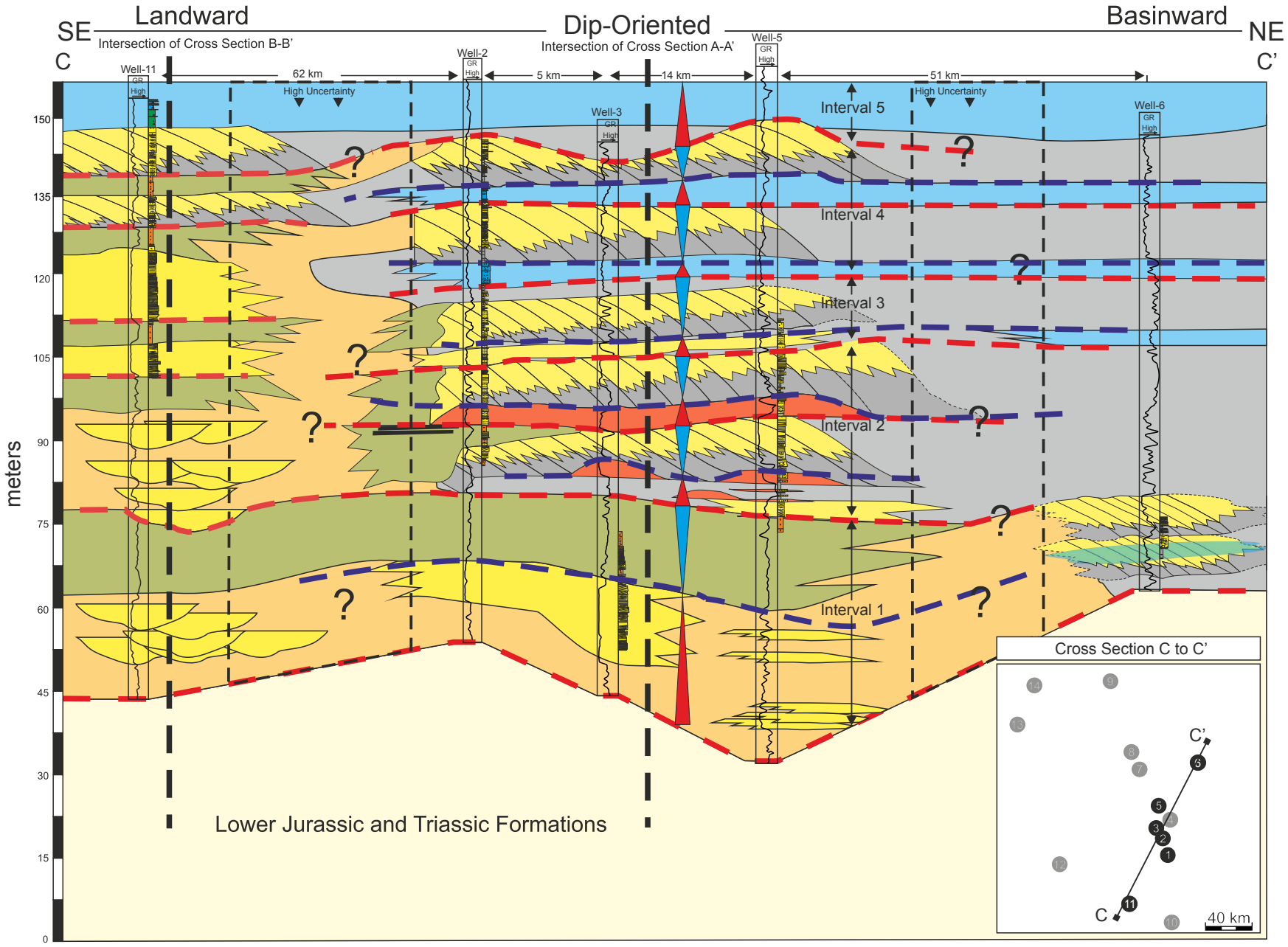
SE
C
Landward
Intersection of Cross Section B-B'
Dip-Oriented
Intersection of Cross Section A-A'
Basinward
NE
C'
Well-11
Well-2
Well-3
Well-5
Well-6
GR
High
62 km
5 km
14 km
51 km
High Uncertainty
High Uncertainty
Interval 5
Interval 4
Interval 3
Interval 2
Interval 1
meters
150
135
120
105
90
75
60
45
30
15
0
Lower Jurassic and Triassic Formations
Cross Section C to C'
C'
C
40 km

Figure 10C

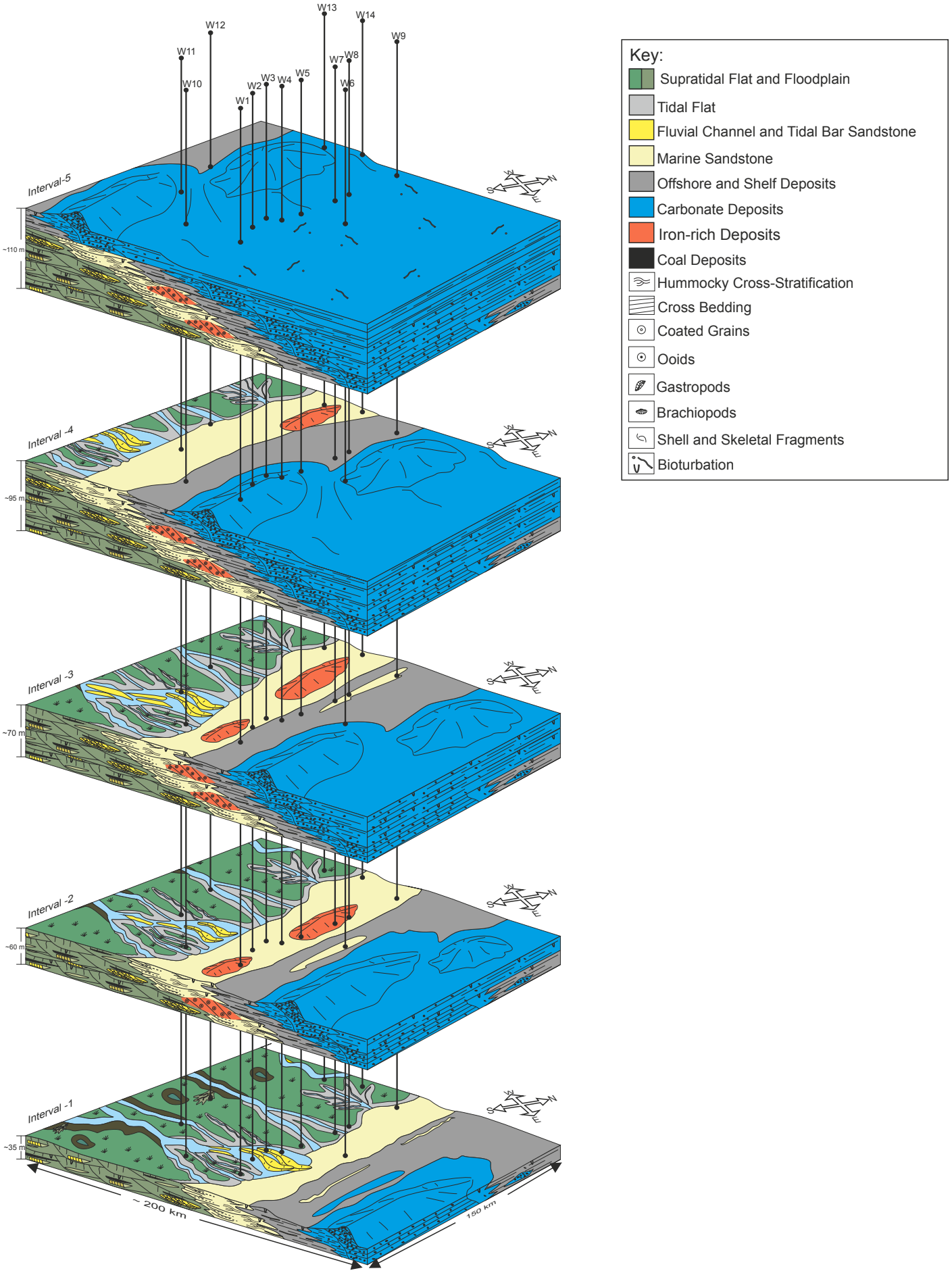
W1
W2
W3
W4
W5
W6
W7
W8
W9
W10
W11
W12
W13
W14
Interval-5
~110 m
Interval -4
~95 m
Interval -3
~70 m
Interval -2
~60 m
Interval -1
~35 m
~ 200 km
150 km
Key:
Supratidal Flat and Floodplain
Tidal Flat
Fluvial Channel and Tidal Bar Sandstone
Marine Sandstone
Offshore and Shelf Deposits
Carbonate Deposits
Iron-rich Deposits
Coal Deposits
Hummocky Cross-Stratification
Cross Bedding
Coated Grains
Ooids
Gastropods
Brachiopods
Shell and Skeletal Fragments
Bioturbation

Figure 11